Water Resources Research

RESEARCH ARTICLE
10.1029/2024WR038455

Special Collection:
Science from the Surface Water and Ocean Topography Satellite Mission

Estimating Channel Parameters and Discharge at River Network Scale Using Hydrological-Hydraulic Models, SWOT and Multi-Satellite Data

Kévin Larnier[1], Pierre-André Garambois[2], Charlotte Emery[3], Léo Pujol[2], Jérôme Monnier[4], Laetitia Gal[1], Adrien Paris[1], Hervé Yesou[5], Thomas Ledauphin[5], and Stéphane Calmant[6]

[1]Hydro Matters, Toulouse, France, [2]INRAE, Aix-Marseille Université, RECOVER, Aix-en-Provence, France, [3]CS Group, Toulouse, France, [4]INSA, IMT, Toulouse, France, [5]SERTIT, ICube, Strasbourg University, Strasbourg, France, [6]IRD, LEGOS, Université Toulouse III, Toulouse, France

Abstract The unprecedented hydraulic visibility of rivers surfaces deformation with SWOT satellite offers tremendous information for improving hydrological-hydraulic models and discharge estimations for rivers worldwide. However, estimating the uncertain or unknown parameters of hydraulic models, such as inflow discharges, bathymetry, and friction parameters, poses a high-dimensional inverse problem, which is ill-posed if based solely on altimetry observations. To address this, we couple the hydraulic model with a semi-distributed hydrological model, to constrain the ill-posed inverse problem with sufficiently accurate initial estimates of inflows at the network upstreams. A robust variational data assimilation of water surface elevation (WSE) data into a 1D Saint-Venant river network model, enables the inference of inflow hydrographs, effective bathymetry, and spatially distributed friction at network scale. The method is demonstrated on the large, complex, and poorly gauged Maroni basin in French Guiana. The pre-processing chain enables (a) building an effective hydraulic model geometry from drifting ICESat-2 WSE altimetry and Sentinel-1 width; (b) filtering noisy SWOT Level 2 WSE data before assimilation. A systematic improvement is achieved in fitting the assimilated WSE (85% cost improvement), and in validating discharge at 5 gauges within the network. For assimilation of SWOT data alone, 70% of data-model fit is in [−0.25; 0.25 m] and the discharge NRMSE ranges between 0.05 and 0.18 (18%–71% improvement from prior). The high density of SWOT WSE enables the inferrence of detailed spatial variability in channel bottom elevation and friction, and inflows timeseries. The approach is transferable to other rivers networks worldwide.

Key Points:

- Saint-Venant model, forced by hydrology, is calibrated via SWOT data assimilation to estimate inflows, bathymetry and friction maps
- Assimilating SWOT alone significantly improves water surface elevation and discharge simulation in the hydrologic-hydraulic model
- Automatic pre-processing of multi-satellite altimetry and images for basin scale model setup and wavelet-based filtering of SWOT L2 RiverSP data at node scale

Correspondence to:
P.-A. Garambois,
pierre-andre.garambois@inrae.fr

Citation:
Larnier, K., Garambois, P.-A., Emery, C., Pujol, L., Monnier, J., Gal, L., et al. (2025). Estimating channel parameters and discharge at river network scale using hydrological-hydraulic models, SWOT and multi-satellite data. *Water Resources Research*, *61*, e2024WR038455. https://doi.org/10.1029/2024WR038455

Received 18 JUL 2024
Accepted 3 JUL 2025

Author Contributions:
Conceptualization: Kévin Larnier, Pierre-André Garambois
Formal analysis: Kévin Larnier, Pierre-André Garambois, Jérôme Monnier
Investigation: Kévin Larnier, Pierre-André Garambois
Methodology: Kévin Larnier, Pierre-André Garambois, Jérôme Monnier
Project administration: Pierre-André Garambois
Software: Kévin Larnier, Charlotte Emery, Léo Pujol

1. Introduction

Improving the estimation of freshwater stocks and fluxes in surface hydrology is crucial for advancing scientific knowledge of the earth system and addressing major socio-economic issues such as water resource management and forecasting extremes (floods and droughts), especially in the context of climate change and potential intensification of the water cycle (Masson-Delmotte et al., 2022). Developing detailed and reliable hydrological-hydraulic (H&H) models that can translate atmospheric signals into river flows, inundations depths, velocities, extents, while integrating available observations, is essential for scientific research and decision support. However, more complex modeling requires more information to constrain it effectively.

Hydrological-hydraulic modeling typically requires data to describe (a) atmospheric forcings, (b) physical properties of the catchment (drainage, topography, land use, soil and bedrock composition, etc) and the hydrographic network (bathymetry, hydraulic friction, structures), as well as flow observations (discharge and water depth at the very least, flow velocities, slopes, soil moisture, etc) to estimate the model parameters. Discharge data, which are crucial to calibrate a stage-discharge law or rainfall-runoff hydrological models, vary in availability depending on the basins and the spatial density of their ground measurement networks. These data integrate the complex signature of combined physical processes occurring in the compartments of the upstream basin (rivers, lakes, biosphere, aquifers and unsaturated soils, cf. Milly (1994)) with significant spatio-temporal variabilities (e.g., Flipo et al. (2014); Schuite et al. (2019)), and contain uncertainty (e.g., Eggleston et al. (2024); Horner et al. (2018); Mansanarez et al. (2016)). Bathymetry and friction data are essential for constraining hydraulic modeling but are often unavailable and remain unmeasurable from space. Dry bathymetry can be accurately measured with airborne LiDAR while wet bathymetry below river surface requires in situ surveys or penetrating

Supervision: Pierre-André Garambois
Visualization: Kévin Larnier
Writing – original draft: Kévin Larnier, Pierre-André Garambois, Jérôme Monnier
Writing – review & editing: Kévin Larnier, Pierre-André Garambois, Charlotte Emery, Léo Pujol, Jérôme Monnier, Laetitia Gal, Adrien Paris, Hervé Yesou, Thomas Ledauphin, Stéphane Calmant

LiDAR in clear, shallow streams (cf. Lague and Feldmann (2020)). Hydraulic model friction can only be estimated indirectly from flow measurements.

Complementing in situ data, new generations of Earth Observation satellites and sensors provide increasingly accurate and spatially dense measurements of water surface (WS) variabilities in worldwide rivers, especially on remote and hard-to-measure areas, including WS elevation Z, width W and slope S.

This hydraulic visibility provided by single or multi-satellite measurements - the potential to depict a hydrological response and surface hydraulic variabilities within a river section or network via remote sensing (Garambois et al. (2017), see also Rodríguez et al. (2020))–can offer valuable information for estimating discharge with local laws or spatialized hydraulic models that both require calibration of their parameters. Local algebraic laws can be stage-discharge rating curves $Q = f(Z)$ (Paris et al., 2016) or width-discharge $Q = f(W)$ (Pavelsky, 2014) or $Q = f(Z, S, W)$ stage-fall-discharge (Malou et al., 2021) or Low Froude Manning-Strickler (Garambois & Monnier, 2015; Larnier et al., 2020). Spatialized hydraulic models can vary in complexity and range from reach scale to network scale (e.g., Coppo Frias et al. (2022); Garambois et al. (2017); Getirana (2010); Paiva et al. (2013); Schneider et al. (2017)).

For instance, the MGB model (Modelo de Grandes Bacias (Collischon et al., 2007; Pontes et al., 2017)), using simplified 1D hydraulics, has been calibrated with ENVISAT data (Getirana, 2010; Paiva et al., 2013) and multi-satellite data (Meyer Oliveira et al., 2021). Other models, such as a simplified 1D hydraulic model of an anastomosed reach (Garambois et al., 2017), a 1D dynamic wave model (Schneider et al., 2017), a low-parameterized steady hydraulic model (Coppo Frias et al., 2022), have been calibrated using various nadir altimetry data. These studies used simplified cross-section (XS) shapes and classical global search algorithms for low-dimensional calibration problems. However, more advanced algorithms are required to estimate high-dimensional, spatially distributed parameters of complete hydraulic models, to approximate flow observations accurately while reducing modeling errors.

Nevertheless, the estimation of hydraulic model parameters from WS observables can result in more or less difficult and ill-posed inverse problems. This difficulty depends on the complexity of the physical system, on the informative content carried by observations, which is linked to their nature and spatio-temporal distribution, on the employed physical model's capability to reproduce partially observed signals from the physical system, and on the sought parameters.

Starting from local physical considerations, at a section or at river reach scale, discharge Q of gradually varied flows (cf. Chow (1959); S. Dingman (2009)) can be related to flow energy slope S_f such that:

$$Q = \kappa S_f^{1/2} = \prod_{i=1}^{N} p_i^{\alpha_i} \tag{1}$$

where κ is the conveyance (S. Dingman, 2009), inversely proportional to a friction parameter ρ such that $p_1 = 1/\rho$ and proportional to the product of the flow parameters p_i raised to the corresponding exponent α_i (cf. S. Dingman (2009); Rodríguez et al. (2020)). Common friction parametrizations include those of Chézy, Manning-Strickler or Darcy–Weisbach (cf. Chow (1959); S. Dingman (2009)). These power laws can be related to rivers hydraulic-geometry (Leopold & Maddock, 1953), see analysis in S. L. Dingman and Afshari (2018); Eggleston et al. (2024) and references therein. Given the relatively large scales of satellite measurements, observed flows can be considered stationary and mainly Low Froude (Fr $\leq$ 0.3), where the friction slope S_f equals the surface slope $S = |\partial_x Z| > 0$. The low Froude Manning-Strickler equation applied with slope S, in its simplest form, (Durand et al., 2014; Garambois & Monnier, 2015) is:

$$Q = KAR_h^{2/3}\sqrt{S} \tag{2}$$

where K is the Strickler friction coefficient, A and R_h are respectivey the wetted flow section and hydraulic radius depending on bathymetry b and XS geometrical shape. Estimating discharge from WS observations with unknown bathymetry b and friction K embedded in the low Froude Manning-Strickler model, is an ill-posed inverse problem (Garambois & Monnier, 2015; Larnier et al., 2020).

When reliable discharge data, from ground-based measurements or calibrated river network models, are available for estimating flow laws parameters, accurate discharge estimates can be achieved. The accuracy of satellite-based discharge estimate depends on observation errors, flow law parameters error and structural model errors Durand et al. (2023); Larnier et al. (2020); Yoon et al. (2016). Site-specific geomorphic and hydraulic conditions affect both ground-based (e.g., Le Coz et al. (2014); Mansanarez et al. (2016)) and satellite-based river flow monitoring (Eggleston et al., 2024; Frasson et al., 2021).

It has been shown that the discharge inverse problem, based on hydrodynamic models and WS measurements without additional priors, is mathematically ill-posed (Larnier et al., 2020). This crucial remark explains the bias observed when using current algorithms for single river portions (see Durand et al. (2023); Frasson et al. (2021) and references therein). The bias depends on the employed physical equations, initial values of iterative algorithms, methodology priors, and other factors (Larnier & Monnier, 2023). The algorithms aiming at calibrating complete space-time dependent flow models (typically Saint-Venant equations based system) need to infer the inflow discharge, bathymetry and friction parameters. After calibration via DA (e.g., assimilation of synthetic SWOT data using variational data assimilation (VDA) (Pujol et al., 2020) or Kalman filter (Wongchuig-Correa et al., 2020)), accurate space-time variations of the signal can be retrieved, albeit with bias. This bias can be removed if considering accurate mean value of discharge or even reference value of one of the two other parameters (bathymetry, friction) as shown in Larnier et al. (2020). Several studies, based on sophisticated VDA processes (Asch et al., 2016; Monnier, 2021) have been developed, see Brisset et al. (2018); Garambois et al. (2020); Gejadze and Malaterre (2017); Gejadze et al. (2022); Larnier et al. (2020); Malou et al. (2021); Oubanas et al. (2018); Pujol et al. (2020) and references therein. A key aspect of these approaches, well-suited for inferring large parameter vectors from heterogeneous data, is starting iterative estimation algorithms with sufficiently accurate initial values. Recent methods define these initial values using probabilistic priors (Gejadze et al., 2022) (inferable from the test data sets itself) or Machine Learning (Larnier & Monnier, 2023). However, these sophisticated strategies face bias issues when dealing with real, imperfect SWOT and/or multi-satellite WS observations and uncertain discharge, bathymetry, and friction. Moreover, these reach-scale discharge estimation approaches may not ensure coherence in inferred discharge patterns across the river network. Therefore, in the context of discharge inversion from satellite data, a basin-scale hydrological-hydraulic modeling approach offers two key advantages: (a) Spatial and temporal coherence of hydrological states and fluxes at the basin scale. (b) Crucial closure for resolving the ill-posed discharge inverse problem using WS observables and a hydraulic model.

The increased spatio-temporal density of Water Surface Elevation (WSE) measurements brought by SWOT, and the visibility of flow lines offer new possibilities to estimate spatio-temporal hydraulic parameters. However, satellite altimetry measurements of WS are relatively sparse in time compared to local flow dynamics. This important aspect of the inverse problem is investigated in Brisset et al. (2018) through identifiability maps comparing available observations and hydraulic wave propagation in space and time, helping to determine the inferrable discharge frequencies (Brisset et al., 2018) or inferable hydrograph time windows (Larnier et al., 2020) at reach scale, for a long reach with several tributaries and using synthetic SWOT data in Pujol et al. (2020). Spatial constraints are also essential, given the generally sparser observation grid compared to the model grid. Spatial regularization is analyzed using synthetic SWOT or nadir altimetry data of different sparsity in Garambois et al. (2020) using HiVDI algorithm (Larnier et al., 2020). Adequate regularizations and spatial scales for parameters must be chosen in the context of spatial equifinality (e.g., Garambois et al., 2020; Pujol et al., 2024), where different parameter spatializations can lead to similar fits to WSE data. The application of VDA to a river network-scale hydraulic model, informed by a hydrological model for flow consistency, would enable maximizing information extraction from available flow observations and estimating physically meaningful parameters.

This study ultimately addresses the following two connected objectives.

- Closing the hydraulic ill-posed inverse problem of inferring river discharge from WS measurements alone. The method builds on the HiVDI algorithm (Larnier et al., 2020; Larnier & Monnier, 2023) but aims to close the ill-posed inverse problem through a (sequential) coupling with a hydrological model over a complete network.
- Improving integrated hydrological-hydraulic (H&H) models of river networks by leveraging the new SWOT data that provide hydraulic visibility for worldwide rivers at unprecedented spatial coverage and resolution.

However, local measurement errors can be significant in some cases. This is complemented by altimetry and imagery from other state-of-the-art satellites to build the prior model geometry.

The developed approach is built on a proposed automatic pre-processing chain and the hydrodynamic solver and dedicated VDA algorithm developed in Larnier and Monnier (2023); Larnier et al. (2020), applied to a complete network. This approach is based on the following ingredients, all applicable to open source data and other basins worldwide:

- A pre-processing algorithm for extracting water surface width (WSW) from optical and radar images, and WSE from ICESat2 altimetry, both used to build the a priori river model geometry.
- A fine analysis and filtering of 1D L2 SWOT river products, using a wavelet-based processing algorithm based on (Montazem et al., 2019) with some upgrades.
- The Saint-Venant hydraulic model posed on a network (open-source computational software DassFlow1D DassFlow (2023)) fed with the discharge values obtained from the pre-calibrated MGB hydrological model (Collischon et al., 2007; Pontes et al., 2017).
- The VDA formulation developed in (DassFlow, 2023; Larnier et al., 2020; Larnier & Monnier, 2023) for the HiVDI algorithm, here applied to the complete network, enables assimilation of multi-source heterogenous data and to estimate high-dimensional spatio-temporal parameters, here the bathymetry, spatially distributed frictions and the inflow hydrographs of the hydraulic model.

The sequential coupling of Hydrology and Hydraulics (H&H) provides a sufficiently accurate initial flow estimate, which is then refined through the VDA process to obtain an (unbiased) accurate space-time variations of the uncertain/unknown fields $Q(x,t), b(x), K(x)$.

After the DA process are obtained: (a) a coherent state-flow modeling over river network at basin scale, (b) sufficiently complex hydraulic modeling to fit high resolution observations of rivers surface deformations.

The remainder of this article is as follows: Section 2 presents the modeling approach and the inverse algorithm, Section 3 presents the studied case and data and processing chain, results and discussions are detailed in Section 4, conclusions and perspectives are given in Section 5.

2. Model and Data Assimilation Algorithm

This section first presents the forward river network model composed of the "differentiable" 1D Saint-Venant hydraulic network model (DassFlow1D) fed with discharges from the semi-distributed hydrological model MGB. It then describes the VDA algorithm, which utilizes cost gradients computed with the adjoint of the hydraulic model. The forward-inverse approach is schematized in Figure 1.

2.1. Hydrological-Hydraulic River Network Model

We consider a 2D river basin domain Ω_{rr} where a spatialized hydrologic model $\mathcal{M}_{rr}$ is applied. This model is here semi-distributed and operates on a mesh composed of topographical sub-basins. Within Ω_{rr}, there is a river network sub-domain Ω_{hy}, composed of connected segments $s = 1..N_{seg}$ between upstream points and successive confluences, where a 1D Saint-Venant $\mathcal{M}_{hy}$ hydraulic model is applied, with inflows being provided by the hydrological model as follows. Subscripts "rr" and "hy" denote rainfall-runoff and hydraulic components respectively.

First, the 1D Saint-Venant hydraulic model for a given river network segment $s \in \Omega_{hy}$ is expressed using the curvilinear abscissa x within segment s and time $t > 0$ as follows:

$$\mathcal{M}_{hy}: \begin{cases} W\dfrac{\partial Z}{\partial t} + \dfrac{\partial Q}{\partial x} & = q_l \\ \dfrac{\partial Q}{\partial t} + \dfrac{\partial}{\partial x}\left(\dfrac{Q^2}{A}\right) & = -gA\left(\dfrac{\partial Z}{\partial x} - S_f\right) \end{cases} \tag{3}$$

where $A(x,t)$ is the cross-sectional area of the flow, $Q(x,t)$ is the volumetric flow rate, $q_l(x,t)$ is the lateral inflow per unit length, g is the acceleration due to gravity, $Z(x,t) = h(x,t) + b(x,t)$ is the WS elevation with water depth

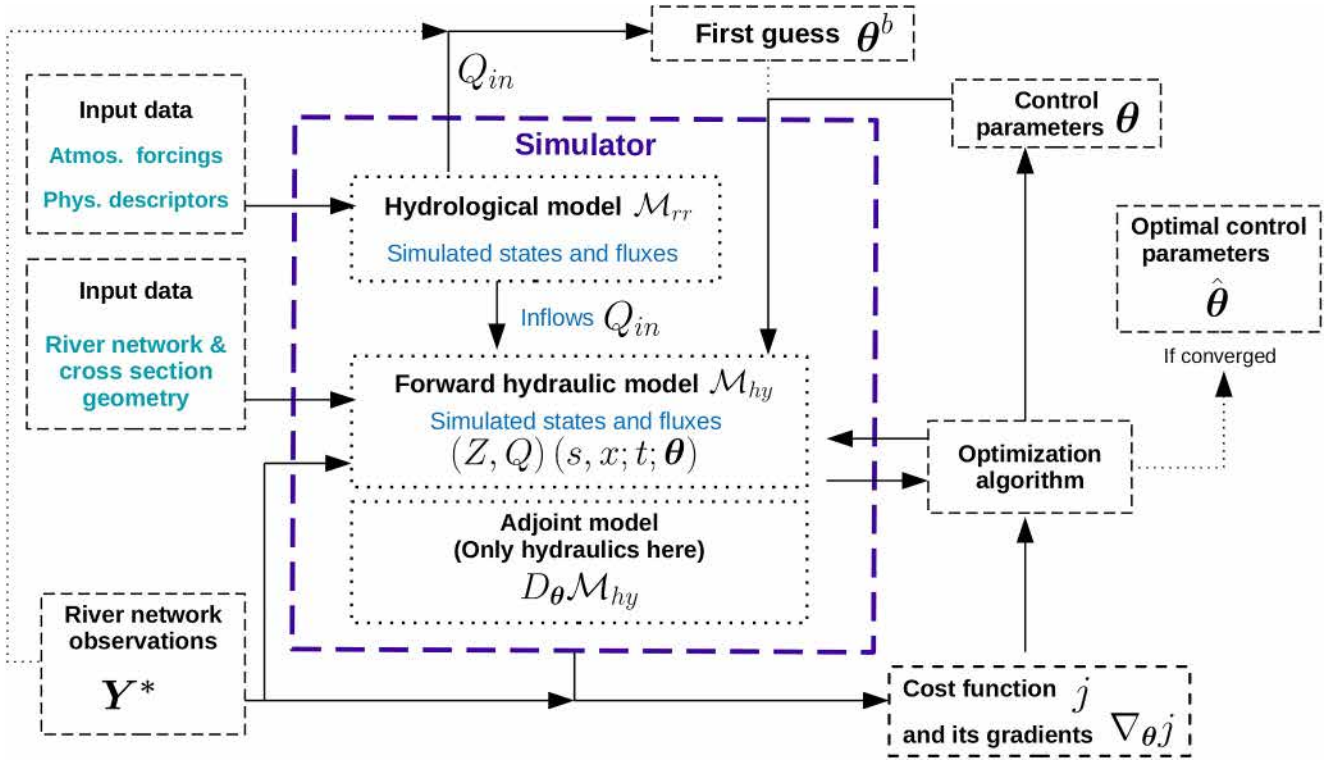

Figure 1. Diagram of the adjoint-based variational data assimilation algorithm (inspired from principle in Monnier (2021)) applied here to the network scale hydraulic model $\mathcal{M}_{hy}$ which inflows are provided by the basin scale hydrological model $\mathcal{M}_{rr}$.

h and bed elevation b, $S_f(x,t) = \frac{|Q|Q}{K^2 A^2 R_h^{4/3}}$ is the Manning-Strickler friction slope with R_h the hydraulic radius and $K(x,h) = \alpha(x)h^{\beta}(x)$ the friction law that is richer than a constant and well-suited for effective 1D modeling of complex flows (e.g., Garambois et al. (2017, 2020)).

This hydraulic model is fed by the hydrologic model $\mathcal{M}_{rr}$ through discharge time series at N_{in} inflow points, with N_{up} upstream and N_{lat} lateral inflow points of the coupling interface $\Gamma_{in} = \Gamma_{up} \bigcup \Gamma_{lat}$, determined by pre-processing as explained later.

Discharge time series simulated by the hydrological model are imposed at upstream boundaries and as lateral mass source terms in the dynamic hydraulic model. This constitutes a weakly coupled hydrological-hydraulic model, denoted as $\mathcal{M} = \mathcal{M}_{hy}(.,.,.;\mathcal{M}_{rr}(.))$, with:

$$\mathcal{M}_{hy} : (K(s;x), b(s;x), Z_{down}(t); (\boldsymbol{Q}_{in}, \boldsymbol{Q}_{lat})(t)) \mapsto (Z, A, Q)(s;x,t) \tag{4}$$

$$\mathcal{M}_{rr} : (\boldsymbol{I}, \boldsymbol{D}) \mapsto (\boldsymbol{Q}_{in}, \boldsymbol{Q}_{lat})(t) \tag{5}$$

where $K(s,x)$ and $b(s,x)$ respectively denote the spatially distributed hydraulic friction coefficient and bathymetry, $Z_{down}(t)$ is the water level time series imposed by satellite altimetry as downstream boundary condition (BC). Additionally, $\boldsymbol{Q}_{in}(t) = Q_{in,1..N_{up}}(t)$ and $\boldsymbol{Q}_{lat}(t) = Q_{lat,1..N_{lat}}(t)$ represent the $N_{in} = N_{up} + N_{lat}$ inflow hydrographs used as upstream BC and lateral source term, respectively, in the hydraulic model $\mathcal{M}_{hy}$ (Equation 3) and predicted by the hydrological model $\mathcal{M}_{rr}$ taking as inputs $\boldsymbol{I}$ and $\boldsymbol{D}$ which are atmospheric forcings and basin physical descriptors (cf. Section 3.2.1). The classical numerical resolution of the hydraulic network model is explained in Appendix A. The subsequent focus will be on the estimation of its parameters.

2.2. Variational Data Assimilation Algorithm

The estimation of spatially and temporally distributed controls (bathymetry, friction, inflow discharges) of the river network hydraulic model is performed from WS observables using the VDA algorithm developed in the so-called HiVDI algorithm, see Larnier and Monnier (2023); Larnier et al. (2020) and to Appendix C. The core principle of this inverse method is to minimize the discrepancy between simulation and observations of river network state dynamics by adjusting the parameter vector $\boldsymbol{\theta}$ of the hydrodynamic model (Section 2.1) starting of a background (first guess) estimate $\boldsymbol{\theta}^{(0)}$. This method is very efficient for optimizing a large and heterogeneous set of hydrodynamic model parameters across an entire river network.

2.2.1. The Sought Unknown Parameter $\boldsymbol{\theta}$

The sought parameter is a large dimensional vector composed of spatially distributed parameters of the hydraulic network model: the friction and bathymetry coefficients over the river network and inflow hydrographs at inflow points. It is defined as:

$$\boldsymbol{\theta} = \left[\left(Q^0_{in,u}, \dots, Q^{T_u}_{in,u}\right)_{u=1..N_{BC}}; \left(b_{1,s}, \dots, b_{N_b(s),s}\right)_{s=1..N_{seg}}; \left(\alpha_s, \beta_s\right)_{s=1..N_{seg}} \right]^T \tag{6}$$

where $Q^{t=1..T_u}_{in,u}$ is the upstream discharge hydrograph imposed at N_{BC} main inflow points (upstream BCs) with T_u discharge values in time (evenly or unevenly discrete hydrograph). The spatialized bathymetry-friction over the river network is as follows: $b_{\square}$ (resp. $\alpha_{\square}$ and $\beta_{\square}$) is the channel bottom elevation (resp. coefficient and exponent of the friction law) with $N_b(s)$ (resp. $N_K(s)$) being the number of bathymetry points (resp. friction patches).

Note that for this study, with the above definition, friction is assumed to be spatially uniform within each segment of the river network. This assumption implies a lower spatial density of friction control compared to bathymetry ones. This is a reasonnable assumption because (a) the friction parameter in the 1D Manning-Strickler parameterization has a rather large meaningful scale, and (b) radar altimetry data used for calibration are heterogeneous and sparser than model resolution (cf. bathymetry-friction spatial patches in Garambois et al. (2020) and large scale applications of the algorithm with lateral inflows from MGB hydrologic model Pujol et al. (2020); Malou et al. (2021)).

The same hypothesis will be used for a parameter estimation experiment with the denser SWOT data in space and time.

2.2.2. Cost Function and Optimization Algorithm

The principle of the VDA algorithm Asch et al. (2016); Larnier et al. (2020); Monnier (2021) is to estimate (discrete) controls of the river network model that minimize the discrepancy between the simulated flow and the available observations. The cost function to be minimized writes:

$$j(\boldsymbol{\theta}) = j_{obs}(\boldsymbol{\theta}) + \gamma j_{reg}(\boldsymbol{\theta}) \tag{7}$$

In this study, flow observations consist in multi-mission altimetric data Z^* heterogeneous in space and time (cf. Appendix B), and the term j_{obs} measures the discrepancy between modeled and observed WS elevations over the hydraulic domain Ω_{hy}:

$$j_{obs}(\boldsymbol{\theta}) = \frac{1}{2}\|Z(\boldsymbol{\theta}) - Z^*\|^2_O \tag{8}$$

The weighted Euclidean norm is defined as $\|x\|^2_O = x^T O x$, with O an a-priori observation covariance operator, here classically a diagonal matrix of constant variance σ_o. (For more details on the introduced covariance operators, we refer to Larnier and Monnier (2023); Larnier et al. (2020)).

Note that $j(\boldsymbol{\theta})$ depends on the control parameter $\boldsymbol{\theta}$ through Z therefore the response of the hydraulic model $\mathcal{M}_{hy}$ (Equation 3) inflowed by the hydrological model $\mathcal{M}_{rr}$, therefore the (sequentially) coupled hydrological-hydraulic model $\mathcal{M}$ (see Equation 4).

The VDA method consists to solve the optimization problem:

$$\hat{\boldsymbol{\theta}} = \underset{\boldsymbol{\theta}}{\operatorname{argmin}} j(\boldsymbol{\theta}) \tag{9}$$

This optimization problem is high-dimensional, say $O(10^4)$. It is solved numerically with the iterative L-BFGS algorithm Bonnans et al. (2006) called in DassFlow (2023)-hence without bounds for parameter search. In DassFlow (2023), the gradient $\nabla_{\boldsymbol{\theta}} j(\boldsymbol{\theta})$ is computed using the adjoint model which is derived by Automatic Differentiation (AD) of the forward code using the AD tool Tapenade Hascoet and Pascual (2013). For further details on the know-hows here implemented, we refer to Monnier (2021); Larnier et al. (2020) and for example, Pujol et al. (2022) for H&H models.

The resulting iterative algorithm is schematized in Figure 1. The first guess value (background value) $\boldsymbol{\theta}^{(0)}$ is defined by inverting the hydraulic model in steady state assuming a geometry shape and friction value, given inflows provided by a pre-calibrated hydrological model. More details are provided the numerical experiments section.

3. Data Processing Chain, Studied Case and Numerical Experiment Design

This sections summarizes the automatic processing algorithms for extracting WSE and WSW from satellite data including both drifting (ICESat-2) and non drifting (Sentinel 3), as well as water masks (either optical or radar) and SWOT filtering. These algorithms are used in conjunction with a preprocessor for hydraulic model meshing and coupling to a precalibrated hydrological model, which is presented next. Finally, the DA experiment plan is outlined.

This study focuses on the Maroni River basin (MRB), in French Guiana, which experiences a tropical climate with distinct rainy and dryer seasons. The study utilizes a diverse and rich data set (Figure 2) processed with new dedicated algorithms before feeding the different components of the forward hydrological-hydraulic model and the VDA algorithm as follows:

- Hydrological modeling (MGB) inputs: physical basin descriptors for semi-distributed mesh of the basin and a priori parameters constrains and hydrometeorological data from worldwide open databases for model setup, discharge at in situ gauges for its calibration (seedetail in Section 3.2.2).
- Hydraulic modeling (DassFlow1D) inputs: A priori river network database and multi-satellite data set of WSE (ICESat2) and WSW (Sentinel) profiles for model geometry construction, inflow discharge from the hydrological model for a priori bathymetry estimation (see Section 3.2).
- Variational Data Assimilation (VDA) inputs: WSE data from Multi-satellites, Sentinel 3 and ICESat2 for spatial density with in situ georeferenced gauges WSE time series for temporal density, or SWOT alone and.

3.1. Water Surface Elevation and Width Processing From Altimetry and Radar Images

WSE data are derived from processed Sentinel 3 data at virtual station (VS) and drifting ICESat-2 ATL13 data using a proposed processing chain. This chain utilizes an a priori water mask and aims to provide hydraulically consistent WSE on XS lines over the river network shapefile (Figure 3, Appendix D).

WSW data are extracted from dynamic water masks using the ExtractEO tool from ICube-SERTIT applied to derive relatively high resolution water masks from Sentinel-1 radar images (cf. Appendix E). These widths (cf. statistics in Figure 4) are used for XS parameterization later. Sentinel data, relatively accurate, is chosen for WSW to enhance information extraction from SWOT WSE data that will be used alone in assimilation.

SWOT data offers remarkable hydraulic visibility but contains measurement errors. We use the SWOT L2 RiverSP product for WSE along river centerlines at a 200 m resolution, applying a wavelet-based filtering and segmentation algorithm following Montazem et al. (2019) (Appendix F). The filtering of SWOT 1-day orbit data is presented in Figure 5, efficiently removes main outliers while depicting multiscale hydraulic information.

The WSE data, whether from altimetry or in situ measurements, are in the same WGS84 vertical reference frame. The observation data set $\boldsymbol{Y}^{*,(0)}$, for determining the prior mesh XS geometry of the hydraulic model, consists of IceSat2 WSE Z^* and Sentinel width W^* on the 2020 years. Three independent assimilation subsets $\boldsymbol{Y}^*$, covering

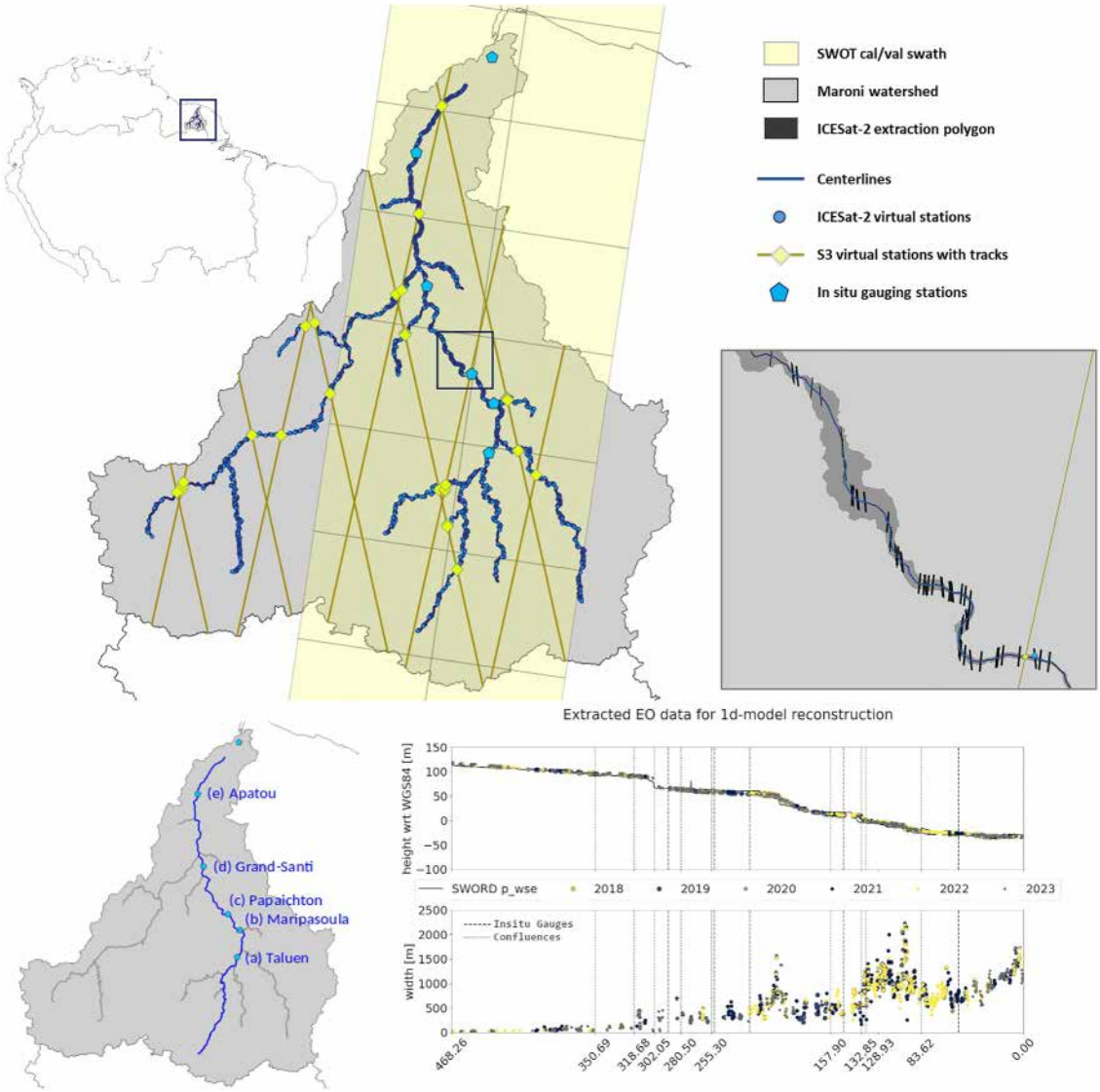

Figure 2. The Maroni River basin in French Guiana with (top) multi-satellite and in situ flow observability over the river network for model building and data assimilation, (bottom) an example of water surface profiles geometry over the Maroni main stream, including elevation data from drifting nadir altimetry (ICESat-2) and width from images (Sentinel 1).

distinct time periods in 2019 or 2023, are composed of altimetry data WSE Z^* from Sentinel and in situ heights, or SWOT data only (Appendix A).

3.2. Maroni H&H Model Construction

3.2.1. Hydrological Model Setup

The hydrological model $\mathcal{M}_{rr}$ used is the MGB semi-distributed model applicable to large tropical bassins (Collischon et al. (2007); Paiva et al. (2013)). Classical preprocessing was applied to obtain flow directions and accumulations based on MERIT-Hydro DEM (Yamazaki et al. (2019)), following the steps outlined in Pontes et al. (2017). Spatial hydrological response unit descriptors on soil and vegetation were derived from FAO HWSD (Nachtergaele et al. (2023)) and ESA WorldCover (Zanaga et al. (2021)), respectively, and converted into 12 HRUs with distinct flow-generation potential. Hydro-meteorological forcings, including climate and rainfall data, were obtained from ECMWF ERA5 data set and GSMAP-RT real-time product (Kubota et al. (2020)). The MGB

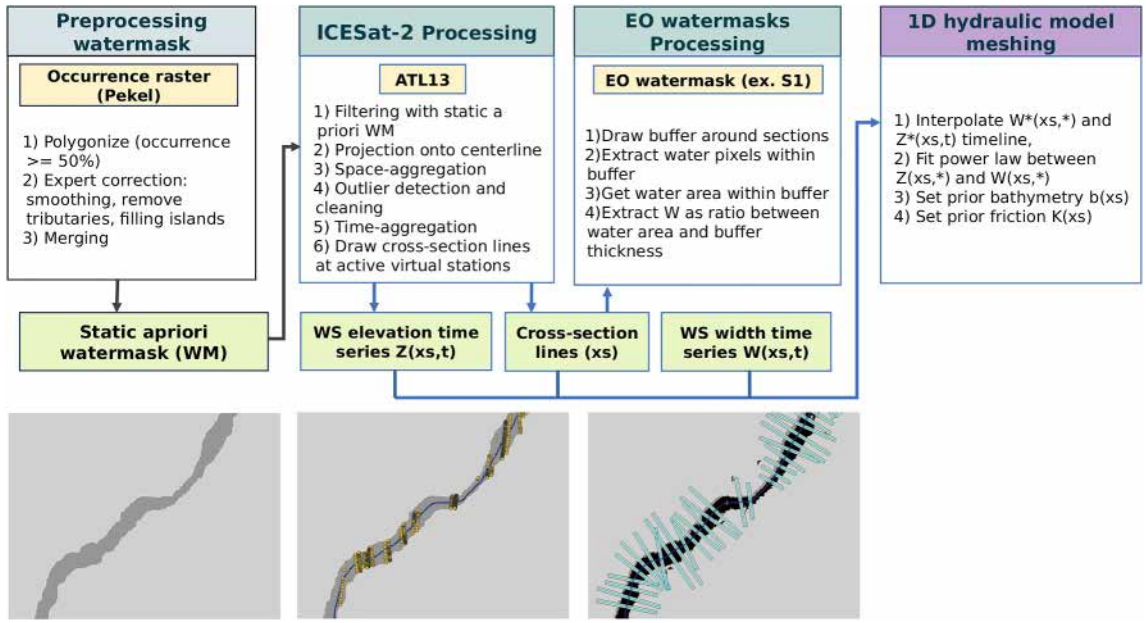

Figure 3. Flowchart of the processing chain for water masks derived from satellite images and ICESat2 altimetry data Z^*, including 1D hydraulic model meshing using cross-sections computed with W^* interpolated on the Z^* timeline.

model is manually calibrated using in situ discharge data with low parameters spatialization. The MRB is divided into 10 sub-basins corresponding to the main tributaries: the Litani, Tampok, Grand Inini, Lawa, Gonini, Upper Tapanahoni, Palumeu, Tapanahoni, Abounami and Maroni. Calibration is performed using observed discharge data from SCHAPI's https://www.hydro.eaufrance.fr/ (accessed on 2024-05-25) at 5 gauging stations: Lawa at Taluen, Tampok at Degrad-Roche, Lawa at Maripasoula, Maroni at Grand-Santi and Maroni at Langa-Tabiki (see Figure 2). The calibration period spans from 2016 to 2023. Calibration is simply performed sequentially from upstream to downstream, considering uniform parameters for each large calibration basin. Ungauged basins are calibrated using the nearest downstream gauge. The discharge simulated, at a daily time step, by the semi-distributed hydrological model are used to feed the hydraulic model at its upstream and lateral inflow boundaries defined below.

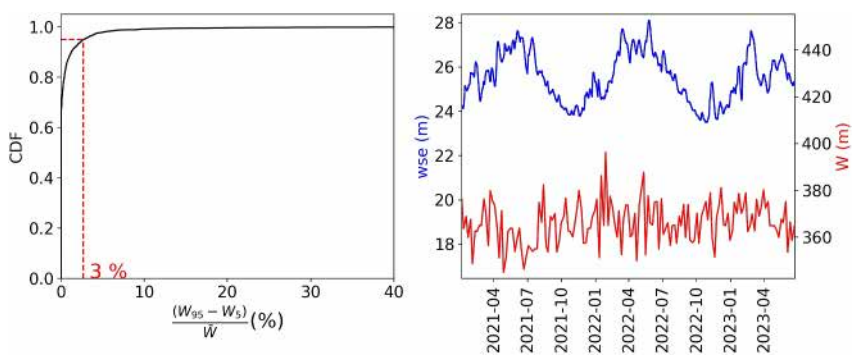

Figure 4. Width variability. (left) Cumulative distributions of relative width variability computed using the 95th and 5th centiles (in order to filter potential noisy extremums), over the whole hydraulic network Ω_{hy} and 2021-01 to 202305 period of temporal water masks, for each cross-section width data are previously filtered to ensure a monotonic increasing relation $W(H)$. 95% of the sections exhibit temporal relative variability lower than 3%. (right) An example from the Papaichton gauging station illustrates the variability of W and H. The timeseries of H and W show no evident correlation ($r^2 = -0.15$, $p = 0.06$), suggesting that the variability in width measurements stems from uncertainties in the computation derived from water masks.

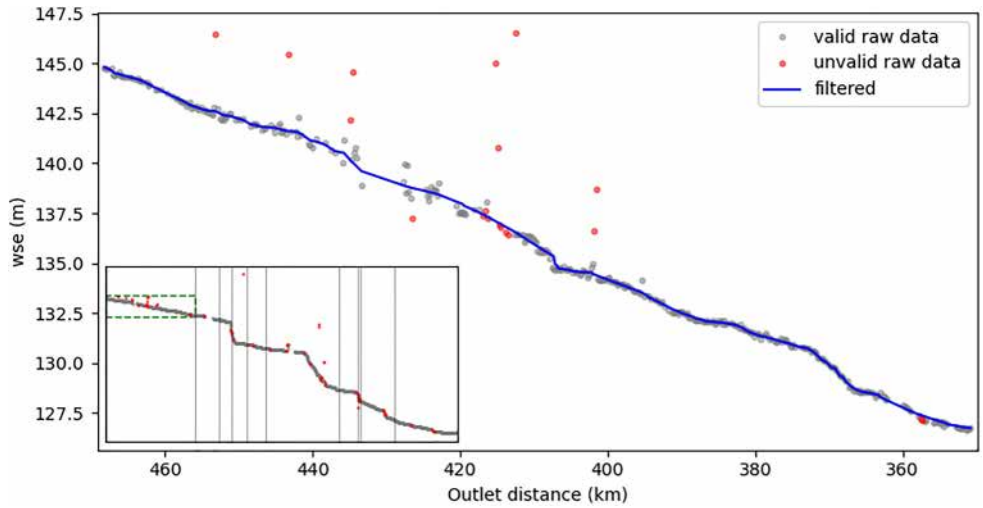

Figure 5. Hydraulic filtering of SWOT L2-RiverSP products at node scale on the main stem for cycle 569 using the pyrscwt algorithm (Python River Segmentation with Continuous Wavelet Transform). The main plot focuses on the first upstream segment of the main stem, displaying the filtered profile as a solid blue line. The inset plot presents the complete main stream, with a dashed green rectangle indicating the zoom area of the main plot, and vertical gray lines marking the segment boundaries, which correspond to main confluences.

3.2.2. Hydraulic Mesh and Coupling With Hydrology

An automatic pre-processing algorithm designed to build coupled hydrological-hydraulic model setup for MGB and DassFlow1D is fed by the multi-satellite data preprocessing chain presented in Section 3.1.

The hydraulic domain Ω_{hy} is determined using the river centerlines from SWORD database Altenau et al. (2021). The downstream boundary is set at Apatou, at a point disconnected from tidal influence because of a sharp river channel bottom variation. Upstream limits are set for rivers draining more than 1500 km^2, based on drainage area obtained from DEM processing. Thus, the hydraulic model covers a long portion of the Maroni main course and many of its tributaries.

Once the hydraulic river network domain Ω_{hy} is determined, the upstream inflow points can be readily identified. In this case, there are $N_{BC} = 12$ such points, where the discharge from the hydrological model serves as BCs for the 1D hydraulic model resolution. Additionally, lateral inflow points are determined, with $N_{lat} = 181$ points identified. Upstream and lateral inflows represent 36% and 50% of the hydrological drainage area respectively. The remaining 14% of mainstream subcatchments were omitted to simplify the coupling process, as their impact is minor compared to other uncertainties in data and modeling within this relatively large, ungauged basin. However, the coupling algorithm should be upgraded to explicitly incorporate inflows from these subcatchments. Additionally, the VDA algorithm and regularization methods will need to be adapted to infer numerous small lateral inflows alongside the spatialized bathymetry, friction, and inflows addressed here. This extension will be the focus of future studies. The hydraulic mesh and coupling points are depicted in Figure 6.

The hydraulic network model $\mathcal{M}_{hy}$ is driven by inflow discharge hydrographs, provided by the pre-calibrated hydrological model $\mathcal{M}_{hy}$. These hydrographs, used as background in DA after, are and denoted $Q^{(0)}_{in,i=1..N_{BC}}(t)$ for upstream inflows and $q^{(0)}_{lat,i=1..N_{lat}}(t)$) for lateral inflows.

3.2.3. Hydraulic Model Geometry

The a priori geometry of the hydraulic model accross the river network is automatically determined from a multi-satellite data set not used in DA experiments: a median water mask $W^{*,50}$ (Sentinel 1 processed with ExtractEO) and a median flow line $Z^{*,50}$ (ICESat2 WSE profiles, cf. Section 3.1), over the period 2019–2021.

In this work, the XS geometry shape of the hydraulic model is defined as rectangular using the median water mask $W^{*,50}$, which is a reasonable assumption, given the relatively limited extent temporal variations observed across

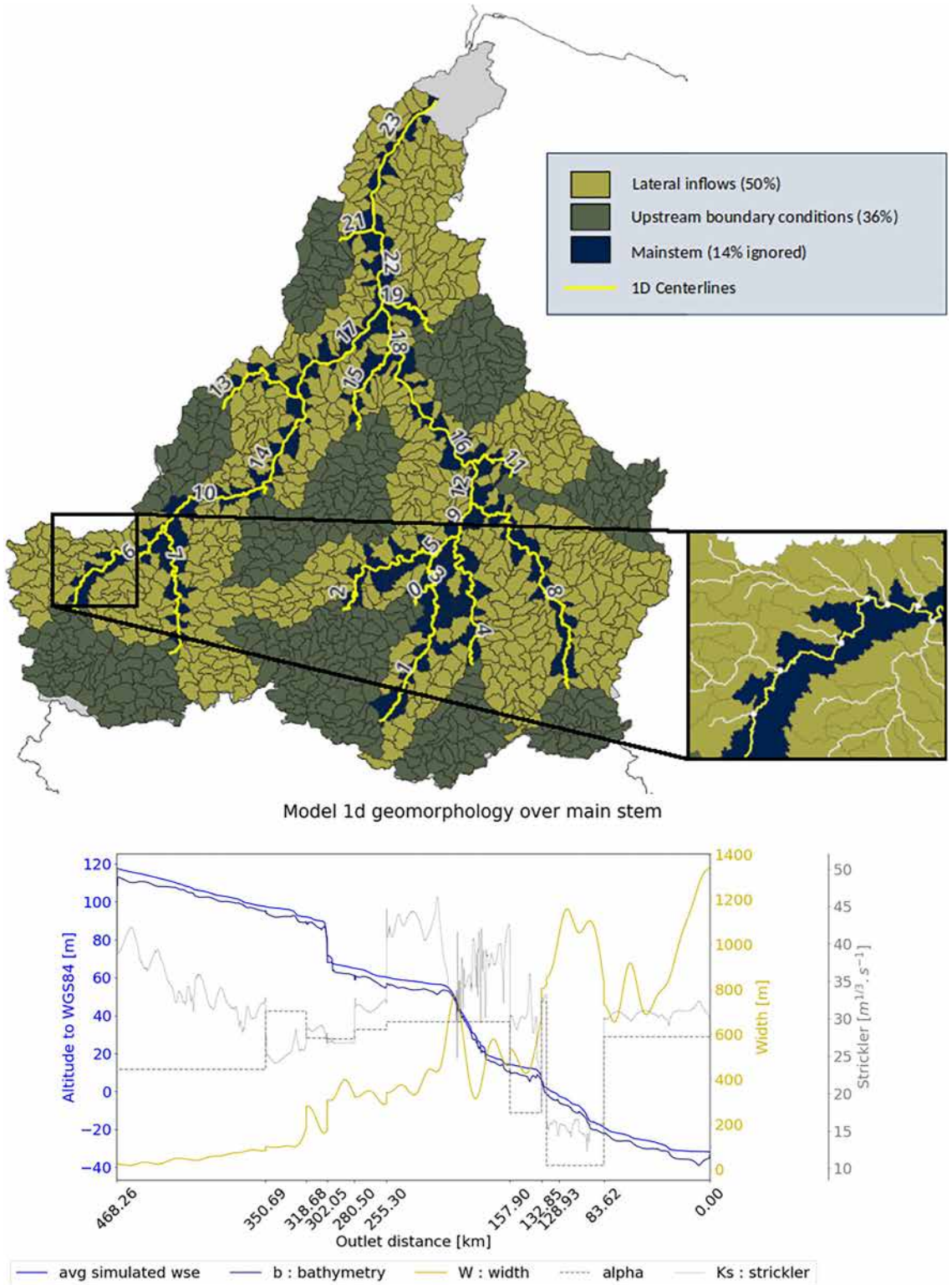

Figure 6. Hydrological-hydraulic mesh with inflow points, percentage of hydrological drainage area given in parenthesis (top). Simulated flow line profile on the Maroni main stream after assimilation of SWOT 1 day data (variational data assimilation experiment "SWOT only"), calibrated bathymetry, and friction profiles $\hat{b}(s,x)$ and $\hat{K}(s,x,\overline{h}) = \hat{\alpha}\overline{h}^{\hat{\beta}}(s,x)$ (gray Strickler axis for α values, note the different unit) for successive connected segments $s = (1,3,5,9,12,16,18,22,23)$ (delimited by main confluences with given abscissas) with $\overline{h}(s,x)$ the average flow line on the studied SWOT time window (bottom).

the entire river network, as shown in Figure 4, and considering the uncertainty in water masks. Furthermore, this rectangular XS shape hypothesis has been sucessfully applied to the "nearby" anastomosed Negro River in our previous studies (Malou et al., 2021; Pujol et al., 2020). It is important to note that the width of this rectangular XS is spatially variable, thereby defining prismatic channels. This variability, combined with the optimized spatially distributed bottom elevation and friction parameters, allows the simulation of complex hydraulic controls (HCs) and their associated nonlinear signatures on the WS profile as shown after. This ultimately results in a good fit to altimetry data and satisfactory discharge inference.

Following the strategy developed in Larnier et al. (2020) (HiVDI algorithm for a single river portion), the background (first guess value) river bed elevation $b^{(0)}_{x,s}$ is obtained by inverting a system based on the Low Froude flow model (Equation 2) at river network scale using: constant friction $K^{(0)} = 30\ \mathrm{m}^{1/3}.\mathrm{s}^{-1}$ (an arbitrary "mild" value for large rivers), a median flow line $Z^{*,50}$ from ICESat2 WSE, and the discharge Q and WS slope S from a steady state forward run of the hydraulic network model fed by median hydrographs (on the corresponding period) of the hydrological model at upstream and lateral inflow points.

This relatively straightforward method enables the determination of a non-trivial bathymetry background $\boldsymbol{b}^{(0)}(x,s)$ with realistic spatial variability accross a river network, using WS observations. This approach is applicable where altimetry data are available, such as spatially dense cross-sections from ICESat-2 here. Figure 6 illustrates this on the main stream of the Maroni River, displaying the mesh granularity, XS width, and bottom elevation variations, including a succession of marked riffles and jumps corresponding to hard rock outcrops. This is one of the river portions over which 1-day orbit SWOT data will be integrated.

Using this background on bathymetry-friction-inflow discharge

$$\boldsymbol{\theta}^{(0)} = \left(Q^{(0),t=1..T_u}_{in,u=1..N_{BC}},\ \boldsymbol{b}^{(0)}_{x,s},\ \alpha^{(0)}_s := 30,\ \beta^{(0)}_s := 0\right) \tag{10}$$

Which is physically meaningfull since it respects the Low-Froude model, the VDA algorithm will seek optimal parameter sets $\hat{\boldsymbol{\theta}}$ of the dynamic hydraulic model, according to the cost function used.

Note that our modeling chain supports the use of more complex geometries, including, a rectangle for wet bathymetry and a superimposition of trapeziums from dynamic water masks (cf. Larnier et al. (2020)). Our algorithm facilitates this complexity, and future research will explore this capability further, with wet bathymetry parameterizations from S. L. Dingman (2007); S. L. Dingman and Afshari (2018) as applied at reach scale in Andreadis et al. (2020).

3.3. Numerical Experiments Design

The Multi-satellite DA experiments utilize the VDA algorithm applied to the coupled hydrological-hydraulic model $\mathcal{M}$ (see Section 2). The numerical experiments aim to demonstrate the potential for simultaneously estimating inflow discharges, bathymetry and friction parameters of the hydraulic model at river network scale from WSE data of varying spatio-temporal density, depending on the scenarios defined later, which presents a significant challenge.

Validation of all experiments considers two key aspects:

- Fit Improvement: The enhancement in fit to WSE compared to the assimilated data set in each case.
- Discharge Time Series: Analysis of discharge time series simulated at internal gauges, which are never assimilated, nor are stage-discharge laws which are implicitly optimized at network scale in the assimilation process via bathymetry and friction fields.

The sought parameter vector $\boldsymbol{\theta}$ of the hydraulic model $\mathcal{M}_{hy}$ is composed of $Q^{t=1..T_u}_{in,u=1..N_{BC}}$ hydrographs at $N_{BC} = 12$ inflows, bathymetry b at $N_b = 2572$ points and friction coefficients α and β at $N_K = 24$ friction patches (i.e., spatially uniform segments). For each DA experiment, the same median WS width W^* is used to define XS geometry over the river network. However, the first guess on bathymetry $b^{(0)}$ varies, as it is computed for different periods using different median inflow discharges and median altimetric flow lines $Z^{*,50}$, following the previously explained method.

The numerical experiment plan, which involves assimilating various combinations of WS altimetry data to infer the previously defined hydraulic parameter vector $\boldsymbol{\theta}$, is as follows:

1. "N4l.2019": Nadir altimetry, drifting IceSat2 and fixed S3 VS, plus 4 in situ WS elevation time series at Maripasoula, Papaichton, Grand Santi and Apatou gauges (with a WGS84 vertical reference in coherence with altimetry, although measurement error sources differ between altimetry and in situ data), over the period 2019/01/01–2019/03/31; (hence b is optimized at those in situ gauges locations); $T_u = 90$ and prior bathymetry is $b^{(0)}_{N4l.2019}$.
2. "N4l.CalVal": Nadir altimetry, drifting IceSat2 and fixed S3 VS, plus 4 in situ WS elevation time series at Maripasoula, Papaichton, Grand Santi and Apatou gauges (with a WGS84 vertical reference in coherence with altimetry), over the period 2023/05/15 to 2023/07/10; (hence b is optimized at those in situ gauges locations); $T_u = 100$ and prior bathymetry is $b^{(0)}_{N4l}$.
3. "SWOT.CalVal": 1-day SWOT orbit data only assimilated over the period 2023/05/15 to 2023/07/10. They cover a large part of the modeled Maroni river network as shown in Figure 2, enabling an evaluation of SWOT's potential for correcting a river network model. $T_u = 100$ and prior bathymetry is $b^{(0)}_{N4l}$.

Note that using in situ WSE time series in "N4l" configurations provides temporally dense information, supplementing the sparser IceSat-2 and Sentinel-3 data. However, it does not provide explicit information on the stage-discharge relationship, which is implicitly sought for the whole river network during assimilation.

The pair of experiments N4l.CalVal and SWOT.Cal/Val can be directly compared, as they both cover the 2023 CalVal period during the peak and recession of a major flood event, offering valuable insight into the inferability of spatio-temporal controls with denser SWOT data. The time period for the first experiment, conducted in 2019 before the SWOT era, was chosen to represent a weaker discharge and a less dynamic hydrological scenario. Therefore, a model spinup strategy will be employed for the second and third experiments. This strategy involves running the forward hydrological-hydraulic model before assimilation to ensure more realistic flow propagation dynamics in the river network, starting the VDA just at the end of a rising limb.

These VDA experiments, initiated from the prior $\boldsymbol{\theta}^{(0)} = \left(Q^{(0),t=1..T_u}_{in,u=1..N_{BC}}, \boldsymbol{b}^{(0)}_{x,s}, \alpha^{(0)}_s \coloneqq 30, \beta^{(0)}_s \coloneqq 0\right)$ with inflows derived from the MGB hydrological model, aim to investigate the constraining power of classical nadir or wide swath SWOT altimetry. The goal is to constrain a hydraulic model of a poorly gauged basin built from remote sensing data. Particular attention will be given to the potential for estimating spatialized channel parameters and inflow hydrographs.

Note that all these inference scenarios correspond to a quasi-ungauged setup for the inversions over the hydraulic network. This means that in situ discharge information within the studied hydraulic domain Ω_{hy} is not considered in assimilation, except indirectly at its boundaries via the inflow discharge from the hydrological model. Specifically, discharge data at in situ gauges were used only for the pre-calibration of the hydrological model. This model provides a priori hydrographs at inflow BCs, and the median discharge in time is used to determine a priori hydraulic bathymetry. In situ discharge time series, which are not assimilated, will be used for analyzing performance after assimilation of WS elevations.The performance will be quantified using the following metrics:

- $NRMSE = \frac{\sqrt{\frac{\sum_{i=1}^{n}(y_i - \hat{y}_i)^2}{n}}}{\bar{y}}$
- $KGE = 1 - \sqrt{(r-1)^2 + (\alpha - 1)^2 + (\beta - 1)^2}$
- $\Delta t_{peak} = \mathrm{argmax}_t\, \hat{y} - \mathrm{argmax}_t\, y$

where y are the observations, $\hat{y}$ the model response, r is the Pearson correlation coefficient, $\alpha = \frac{\sigma_{\hat{y}}}{\sigma_y}$ and $\beta = \frac{\bar{\hat{y}}}{\bar{y}}$.

For every experiment, the parameters of the background error covariance matrix B, used in the VDA algorithm and influencing the optimal solution $\hat{\boldsymbol{\theta}}$, are set a priori from physical considerations as investigated in Garambois et al. (2020); Larnier et al. (2020); Pujol et al. (2020). The parameters L_Q and L_b act as correlation length in space and time, respectively, while the $\sigma_{\square}$ may be viewed as variances. Given the typical low Froude number of the flows at the observation scale and hydrological frequencies for this large basin, adequate values for these parameters are:

$\left(\sigma_{Q_{in,i}} = 0.01\,\bar{Q}^{(0)}_{in,i}\right)_{i=1,N_{BC}}$, $L_Q = 10$ days, $\sigma_b = 0.1$ m, $L_b = 200$ m, $\sigma_\alpha = 0.5$ m$^{1/3}$.s^{-1} and $\sigma_\beta = 0.01$.

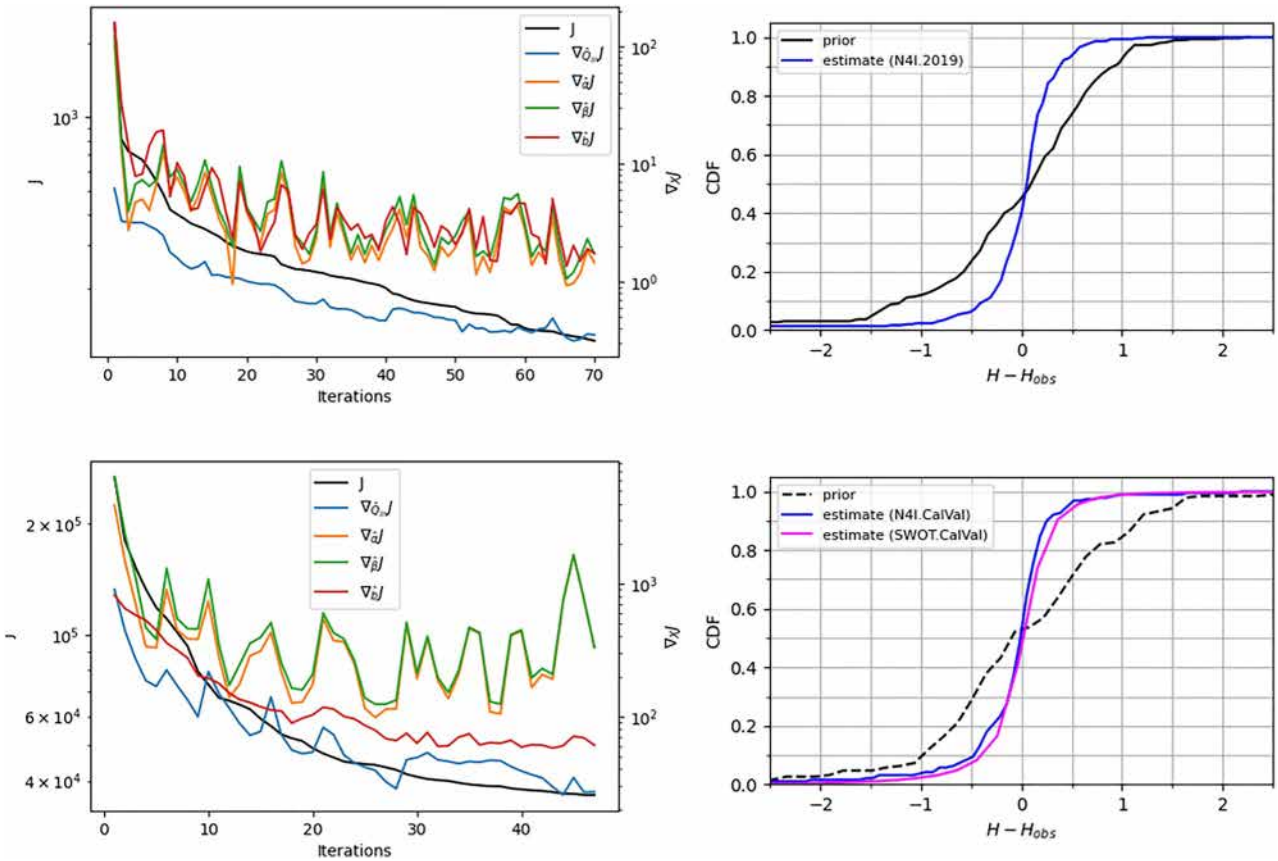

Figure 7. (left) Convergence curves of cost J (Equation 7) and evolution of its gradients $\nabla_{\square}$ with respect to the sought spatio-temporal parameters. (right) cumulative distribution function of absolute misfit of simulated water surface elevation (WSE) to altimetry data which are assimilated in meters for "prior" (background) $\hat{\boldsymbol{\theta}}^{(0)}$ and calibrated parameters $\hat{\boldsymbol{\theta}}_{\square}$. Model misfit values are as follows: (top) "N4l.2019" (8,928 space time points from nadir altimetry and in situ WSE) 88% in (−0.5, 0.5)m, 69% in (−0.25, 0.25)m, the $5-th$ and $95-th$ percentiles of errors are $\epsilon_{Q5} = -0.6$ m, (resp. $\epsilon_{Q95} = 0.53$ m), respectively; (bottom) "NAl.CalVal" (5,467 space time points from nadir altimetry and in situ WSE), 87% in (−0.5, 0.5)m, 68% in (−0.25, 0.25)m, the $5-th$ and $95-th$ percentiles of errors are $\epsilon_{Q5} = -0.9$ m and $\epsilon_{Q95} = 0.45$ m, respectively; and "SWOT.CalVal" (179,192 space time points from SWOT only), 88% in (−0.5, 0.5)m, 68% in (−0.25, 0.25)m, the $5-th$ and $95-th$ percentiles of errors are $\epsilon_{Q5} = -0.6$ m and $\epsilon_{Q95} = 0.52$ m, respectively.

The solvability of the inverse problem (9) obviously depends on the available data, their nature, and their space-time density versus the nature and dimension of the inferred parameter θ. On the concept of identifiability in the present hydraulics context, we refer to Brisset et al. (2018), which highlights key concepts for assessing the solvability of the treated inverse problem or not and the inferrable hydrograph frequencies. In the present multi-physics network configuration, we have decided to first focus on the identifiability of the upstream inflows of the hydraulic network model, without considering the lateral ones (the latter being given by the hydrological model). Pujol et al. (2020) shows that the simultaneous inferrence of lateral inflows and channel parameters can be done, however it was on a single (long) reach. Adding the lateral inflows to the uncertain parameters (in the vector θ) using the considered data set and the present H&H model in addition to the bathymetry and friction parameters over a river network, should be investigated in a future study.

4. Results and Discussions

The overall performances, both in terms of fit to the WSE data used in calibration (either nadir altimetry and in situ WSE for N4l, or SWOT data alone) and the reproduction of discharge at gauging stations within hydraulic domain Ω_{hy} (not used in assimilation), is very satisfactory for the three VDA experiments (Figure 7). Notably, there is a very significant improvement in the fit to observed WSE over the spatio-temporal domain, with errors reduced to below 0.5 m. This improvement of the simulated WSE profiles, in terms of relative cost improvement

$\left[J(\boldsymbol{\theta}_{\square}^{(0)}) - J(\widehat{\boldsymbol{\theta}_{\square}})\right]/J(\boldsymbol{\theta}_{\square}^{(0)})$ is of 95% for "N4l.2019," 93% for "N4l.CalVal" and of 86% for "SWOT.CalVal," which has a much denser data set.

The performance in terms of simulated discharges at validation gauges (discharge is not assimilated, only WSE in N4l configuration) within the river network is also very satisfactory with significant improvements from prior $\boldsymbol{\theta}_{\square}^{(0)}$ to inferred $\widehat{\boldsymbol{\theta}_{\square}}$ model parameters. The NRMSE improvements from the prior range from:

- 32%–76% for "N4l.2019" (with values in 0.09–0.23).
- 29%–71% for "N4l.CalVal" (with values from 0.06 to 0.22) and from 18% to 71% for "SWOT.CalVal" (with values from 0.05 to 0.18).

These improvements, both in fitting the assimilated WSE and in predicting unseen discharge timeseries at internal gauges for two distinct time periods with different hydrological responses, validate the method. This is achieved by simultaneously optimizing bathymetry, friction across the entire river network, and upstream inflow hydrographs from WSE only. Notably, WSE time series at gauges are not assimilated in "SWOT.CalVal" which is compared to "N4l.CalVal." A detailed analysis of the results from the three DA experiments is provided after. The analysis covers the fit to the assimilated *WSE* observations, validation against in situ discharge timeseries at gauges, and correction of the hydraulic parameters.

4.1. Multimission Nadir Altimetry and In Situ WSE Assimilation 2019 (N4l.2019)

This analysis focuses on the assimilation experiment "N4l.2019," which integrates S3 and ICESat2 nadir altimetry data along with in situ WSE at the four in situ gauges.

Figure 7 presents the minimization of the cost function and its gradients to the sought spatialized parameters, along with the fit to WSE data of the model before $\mathcal{M}(\boldsymbol{\theta}_{N4l}^{(0)})$ and after $\mathcal{M}(\hat{\boldsymbol{\theta}})$ calibration. The fit of WSE is significantly improved from the background prior parameters $\boldsymbol{\theta}_{N4l}^{(0)}$ to the control $\hat{\boldsymbol{\theta}}$ estimated by VDA of WSE. The simulation error on WSE is within (−0.5, 0.5)m for 88% of the data points, and within (−0.25, 0.25)m for 69% of the data points. The $5-th$ and $95-th$ percentiles of the errors are $\epsilon_{Q5} = -0.6$ m and $\epsilon_{Q95} = 0.53$ m, respectively.

This represents a significant improvement in the fit to the spatio-temporally heterogeneous WSE data used in calibration. Interestingly, this also results in a significant improvement in the simulated discharge at the gauging stations within the hydraulic domain Ω_{hy}, as evidenced by Figure 8 and Table 1 (final NRMSE between 0.08 and 0.19). It is important to note that discharge data were not used in this calibration; only WSE data from four out of five gauges were used, with gauge section bathymetry and friction inferred.

The data assimilated in "N4l.2019" consist in relatively sparse WSE over the spatio-temporal domain (284 satellite altimetry points over the network) with some temporal density provided by WSE at the four gauges (2,161 WSE values per gauge, totaling 8,644). This is compared to the size of the sought spatio-temporal controls. Internal discharge prediction is improved after assimilation of WSE, compared to the prior hydraulic model, at all gauges which are located along the Maroni main stream. This improvement results from the correction of hydraulic model controls which pertain to spatialized channel bathymetry-friction and hydrographs at $N_{BC} = 12$ upstream inflow points.

Those satellite-based estimates of mass fluxes and river network bathymetry-friction parameters $\hat{\boldsymbol{\theta}}_{N4l}$, at the upstream boundaries Γ_{up} and over the river network hydraulic domain Ω_{hy} are summarized in Figure 9. Significant corrections of bathymetry-friction are obtained for most segments of the river network. These corrections, along with adjustments of upstream inflow corrections (see inferred inflows hydrographs and bathymetry profiles in appendix Appendix G), improve the fit of the simulated flow line to local altimetry and in situ WSE data. Several factors contribute to the complexity of the influence of these hydraulic parameters on the simulated flow line trough the hydraulic model:

- Upstream to downstream propagation: the inflow discharge propagates and aggregates along the river network. Only upstream BCs on Γ_{up}, representing 50% of basin area as shown by Figure 6, are corrected here.
- Local competition between bathymetry and friction: These parameters are embedded in the friction source term S_f of the 1D Saint-Venant (Equation 3).

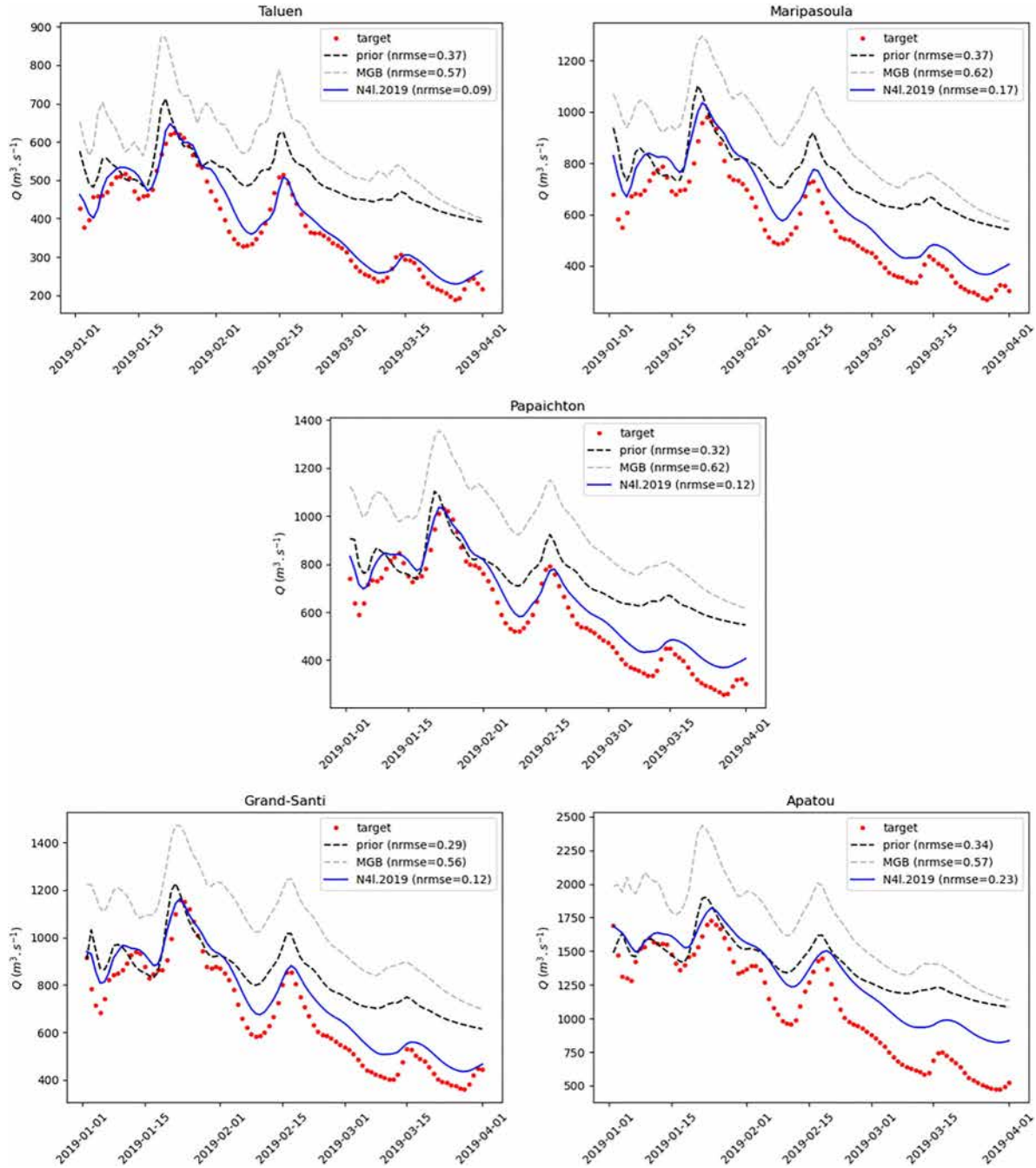

Figure 8. Validation of the calibrated Saint-Venant river network model on 2019 period: simulated discharge at internal gauges along the Maroni main stream following the assimilation of nadir altimetry (Sentinel 3 and ICESat-2) and in situ water surface elevation at (excluding Taluen) in the "N4I.2019" experiment. The nRMSE ranges from 0.09 for the Taluen station to 0.23 for the Apatou (most downstream) station.

- Downstream controls: complex correlated influence of the sought HCs toward upstream on so called back-water length under the fluvial regime studied (see Montazem et al. (2019); Samuels (1989)).

In essence, the inverse problem of estimating most flow controls (except lateral inflows) of the network Saint-Venant model is challenging due to local equifinality and spatial equifinality. A satisfying solution was achieved thanks to a realistic prior on the sought parameters and the regularizations introduced via covariances matrices (cf. Section 2.2.2). A more detailed hydraulic analysis of the inferred local HCs, along with discussion on the controllability of hydrological inflows, is made after.

Table 1
Performance Metrics at Gauges Stations for the N4l.2019 Experiment

	Prior			MGB			Inferred		
Gauge	NRMSE [-]	KGE [-]	Δt_{peak} [days]	NRMSE [-]	KGE [-]	Δt_{peak} [days]	NRMSE [-]	KGE [-]	Δt_{peak} [days]
Taluen	0.37	0.45	−2	0.57	0.43	−3	0.09	0.94	−1
Maripasoula	0.37	0.52	−2	0.62	0.39	−1	0.17	0.84	−1
Papaichton	0.32	0.51	−2	0.62	0.38	−1	0.12	0.85	−1
Grand-Santi	0.29	0.56	−1	0.56	0.44	−1	0.12	0.88	0
Apatou	0.34	0.43	−1	0.57	0.42	−2	0.23	0.70	0

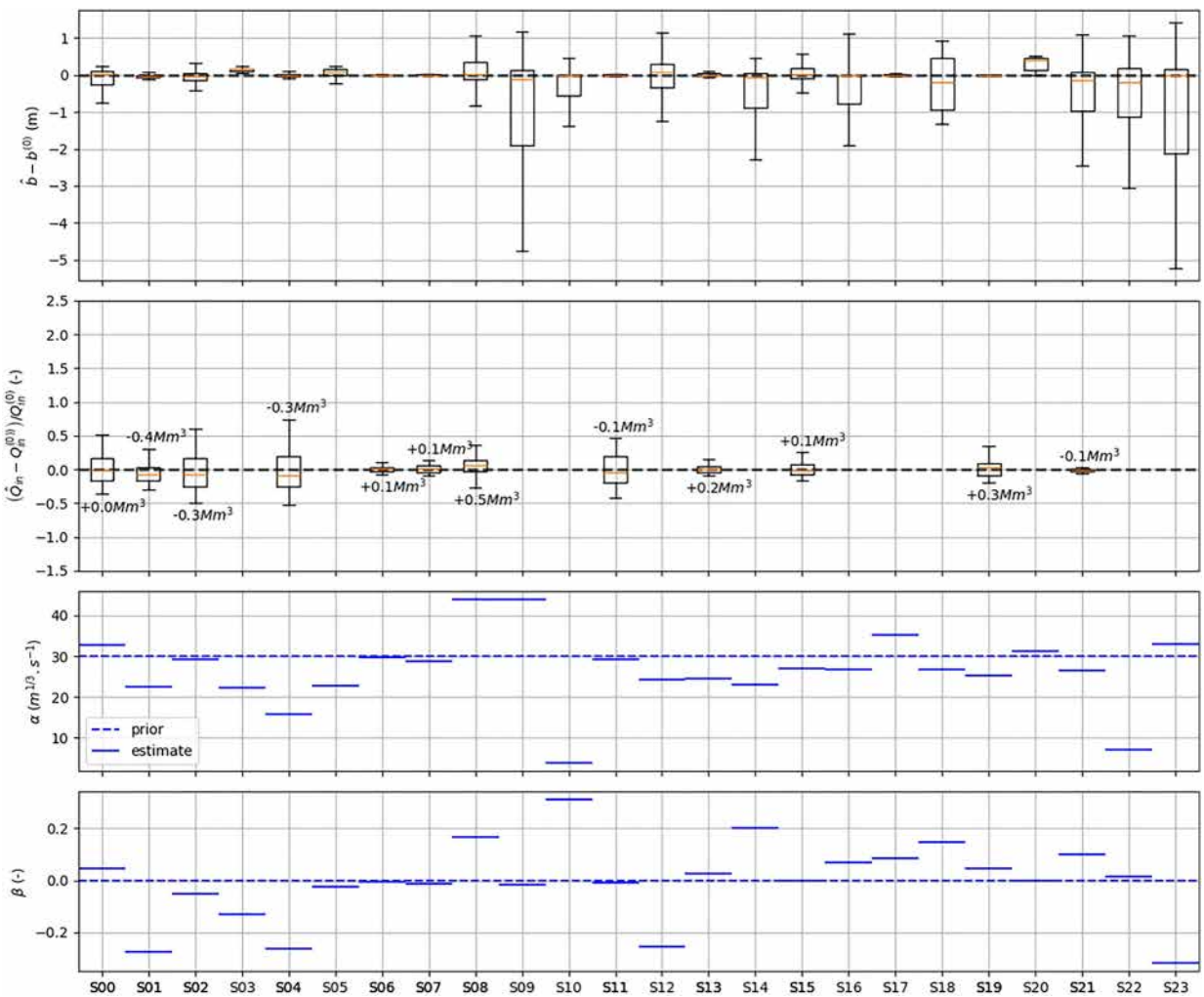

Figure 9. Relative correction of hydraulic model parameters after assimilation of nadir altimetry and in situ water surface elevation data in the experiment "N4l.2019." The figure shows inferred parameters $\hat{\boldsymbol{\theta}}$ by variational data assimilation from the background $\boldsymbol{\theta}_{N4l}^{(0)}$, represented by river network segment "S00" to "S23." (top) boxplots of spatially distributed corrections of bathymetry $b(s,x)$ at $N_b = 2,572$ hydraulic cross sections and of (second) inflow discharge hydrographs $Q_{in,u=1..N_{BC}}^{t=1..T_u}$ at $N_{BC} = 12$ inflows,(third and fourth) friction parameters $\hat{\alpha}$ and $\hat{\beta}$ across the 24 segments composing the simulated river network.

4.2. SWOT CalVal 1-Day Orbit (SWOT.CalVal and N4l.CalVal)

This analysis focuses on the assimilation experiment of "SWOT.CalVal," which utilizes wide swath altimetry data from track #007 during fast sampling (cal-val) orbit. This data covers a large area of the Maroni basin, including the main stream "along track" with a 1 day repeat cycle. The results of the "SWOT.CalVal" experiment are compared with the "N4l.CalVal" experiment, which assimilates S3 and ICESat2 nadir altimetry data along with in situ WSE data over the same time period.

The time period from 2023 to 05-15 (start of consolidated SWOT measurements) to 2023-07-10, covered by SWOT's 1 day orbit data, corresponds to the peak and declining limb of a relatively strong flood: the estimated peak flow in May 2023 at Apatou downstream of the basin is above $4,500\ \mathrm{m}^3/\mathrm{s}$. Therefore, a warmp up period is used to obtain a physically meaningfull initial state in the river network for starting assimilation (cf. details in Section 3.3). Note that a wavelet-based filtering algorithm is systematically applied to remove outliers in SWOT data (cf. Figure 5) before VDA.

Figure 7 presents the minimization of the cost function and its gradients to the sought spatialized parameters, along with the fit to SWOT WSE data of the model before $\mathcal{M}(\boldsymbol{\theta}^{(0)}_{SWOT})$ and after $\mathcal{M}(\hat{\boldsymbol{\theta}})$ calibration. The fit of WSE is significantly improved from background prior parameters $\boldsymbol{\theta}^{(0)}_{SWOT}$ or $\boldsymbol{\theta}^{(0)}_{N4l}$ to the control $\hat{\boldsymbol{\theta}}$ estimated by VDA of WSE respectively for SWOT or nadir and in situ.

For "SWOT.CalVal," the simulation error on WSE is within $[-0.5, 0.5]$m for 88% of the data points, within $(-0.25, 0.25)$m for 68% of the data points. The errors for the $5-th$ and $95-th$ percentiles are $\epsilon_{Q5} = -0.6$ m and $\epsilon_{Q95} = 0.522$ m respectively. A comparable improvement in fit to nadir altimetry and in situ WSE is also obtained in "N4l.CalVal" configuration, with a simulation error on WSE within $(-0.5, 0.5)$m for 87% of the data points and within $(-0.25, 0.25)$m for 69% of the data points. The $5-th$ and $95-th$ errors percentiles are are $\epsilon_{Q5} = -0.9$ m and $\epsilon_{Q95} = 0.46$ m respectively.

This represents a significant improvement of the fit to SWOT WSE used in calibration, that are 600 times denser in space and time than nadir altimetry and in situ data used in "N4l.CalVal" experiment (179,192 data points in space and time with SWOT compared to 5,467 for nadir altimetry and in situ WSE). The similar fit obtained in the two configurations highlights the strength of our approach for integrating heterogeneous data of different sparsity.

Interestingly, over the shorter time window studied here and this assimilation of SWOT data only in "SWOT. CalVal," or of nadir altimetry and in situ WSE in "N4l.CalVal," both result in an improvement of the discharge (not assimilated, challenging to estimate) simulated at gauging stations within the hydraulic domain Ω_{hy} (cf. Figure 10 and Table 2). Both experiments lead to significant discharge improvements at internal gauges. The NRMSE on discharge at those internal gauges ranges in $[0.05;0.18]$ for "SWOT.CalVal" and $[0.06;0.22]$ "N4l. CalVal" while prior discharge nrmse is in $[0.17;0.34]$. This further validates our approach, using WSE data from different altimetry missions and in combination or not with in situ WSE.

This improvement in terms of internal discharge, but also of the fit to the WSE assimilated, represent a good result for this challenging inference in the declining limb of a strong flood not reproduced by the hydrological model (gray dashed hydrographs) hence providing unfavorable prior inflows for VDA (black dashed hydrographs simulated by $\mathcal{M}(\boldsymbol{\theta}^{(0)}_{SWOT})$ with both under and over estimations of real discharge which is a challenging case for VDA).

Moreover, for each gauge, comparable discharge improvements are obtained between the two experiments, in part because they are started from similar discharge background (but different prior bathymetry). But above all this outlines that sufficient information is contained in both altimetry data sets to constrain the sought parameters of the hydraulic model over the river network.

The optimized parameter $\hat{\boldsymbol{\theta}}_{SWOT}$, including inflow discharge hydrographs, spatialized bathymetry and friction over the river network hydraulic domain, are summarized in Figure 11 for the "SWOT.CalVal" experiment. (Note: Controls for the "N4l.CalVal" experiment are detailed in the Appendix G). Again, for most segments of the river network, substantial corrections of bathymetry and friction are obtained. Note that the calibrated friction coefficient α generally ranges between 10 and 40 $\mathrm{m}^{1/3}\cdot\mathrm{s}^{-1}$, although a few reaches exhibit higher or lower values. These are effective parameters that work in conjunction with other optimized controls of the hydraulic model- bathymetry and inflows. These adjustments enable an improved fit of simulated flow to altimetry and in

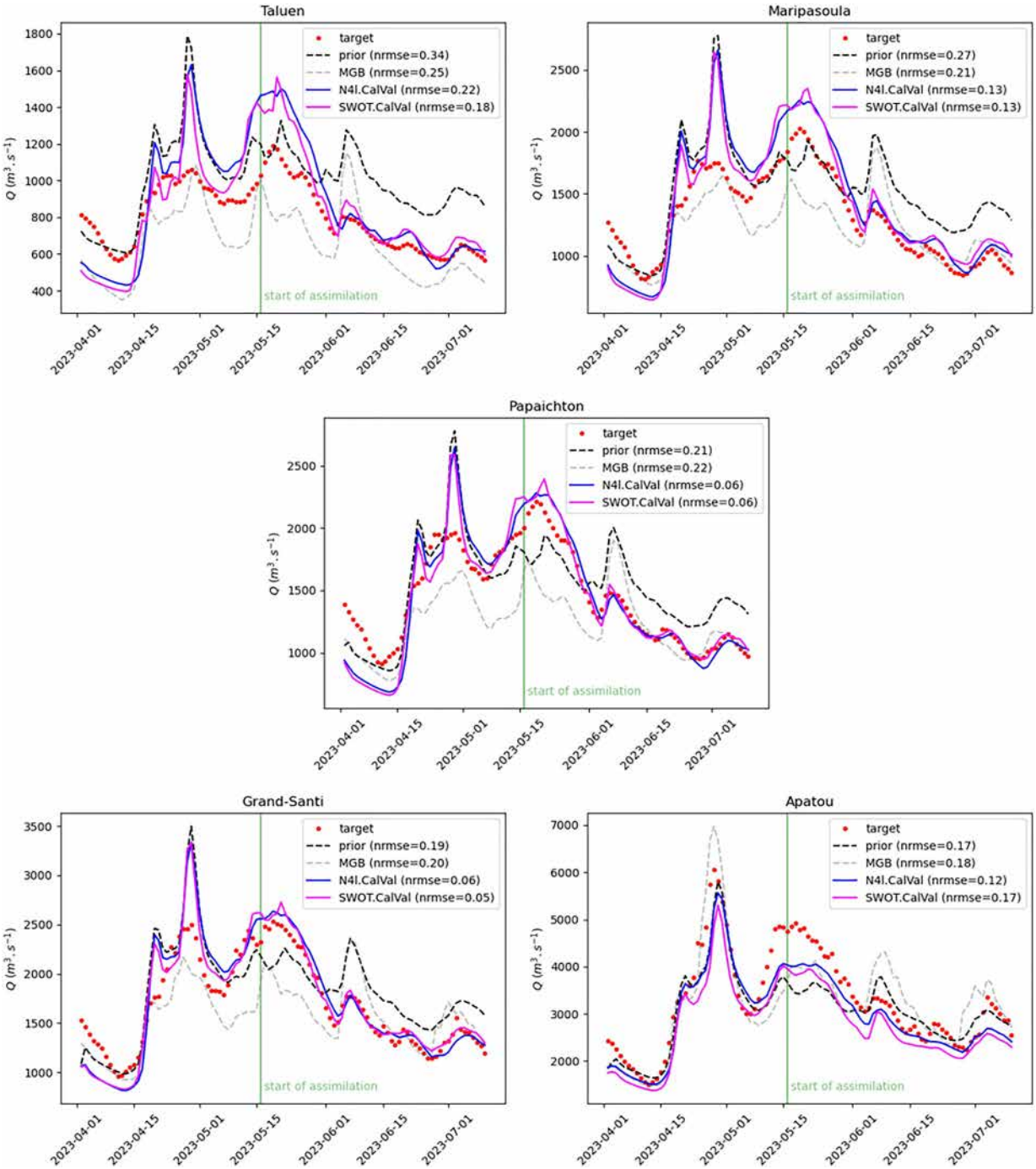

Figure 10. Validation of the calibrated Saint-Venant river network model on CalVal period in 2023: simulated discharge at internal gauges along the Maroni main stream following the assimilation over the Maroni Network of SWOT 1 day altimetry or nadir altimetry and in situ water surface elevation data in N4l configuration. The nRMSE ranges from 0.06 at the Grand-Santi and Papaichton stations to 0.22 at the Taluen station for the N4l.CalVal experiment and from 0.05 at the Grand-Santi station to 0.18 at the Taluen station for the SWOT.CalVal experiment.

situ WSE data. Recall that inferring these parameters from WSE data- which pertains to all controls of a 1D Saint-Venant hydraulic model- involves dealing with local structural equifinality (due to parameters embedded into friction term S_f and having a correlated influence on simulated WS) and spatial equifinality, as analyzed in Garambois and Monnier (2015); Garambois et al. (2020); Larnier et al. (2020); Pujol et al. (2024). To address this ill-posed inverse problem, covariance matrices are used in the VDA algorithm (as for previous "N4l.2019"

Table 2
Performance Metrics at Gauges Stations for the N4l.CalVal and SWOT.CalVal Experiments

		Prior			MGB			Inferred		
Exp.	Gauge	NRMSE [-]	KGE [-]	Δt_{peak} [days]	NRMSE [-]	KGE [-]	Δt_{peak} [days]	NRMSE [-]	KGE [-]	Δt_{peak} [days]
N4l.CalVal	Taluen	0.34	0.54	2	0.25	0.66	−3	0.22	0.30	2
	Maripasoula	0.27	0.52	2	0.21	0.56	−2	0.13	0.74	0
	Papaichton	0.21	0.52	2	0.22	0.54	−2	0.06	0.84	0
	Grand-Santi	0.19	0.54	3	0.20	0.53	−2	0.06	0.87	0
	Apatou	0.17	0.44	−2	0.18	0.54	5	0.12	0.76	2
SWOT.CalVal	Taluen	0.34	0.54	2	0.25	0.66	−3	0.18	0.49	1
	Maripasoula	0.27	0.52	2	0.21	0.56	−2	0.13	0.77	2
	Papaichton	0.21	0.52	2	0.22	0.54	−2	0.06	0.87	2
	Grand-Santi	0.19	0.54	3	0.20	0.53	−2	0.05	0.92	2
	Apatou	0.17	0.44	−2	0.18	0.54	5	0.17	0.72	−2

experiment) to achieve a regularizing effect. This effect includes preconditioning and spatial or temporal regularization, smoothing the estimated spatial or temporal quantities when they are denser than observations.

The inferred hydrographs and bathymetry-friction profiles for each segment of the network are shown in appendix Appendix G. Detailed spatial parameters variabilities can be inferred thanks to the spatial density of SWOT data, which will be analyzed and compared to the inference with the nadir altimetry WSE data.

4.3. Detailed Analysis of Inferred Parameters

The inferences of spatio-temporal parameters for the river network hydraulic model were performed from 2 data sets with significantly different spatio-temporal density, with the SWOT data set being much denser in space and time. The bathymetry-friction profiles inferred over the Maroni main stream, specifically fo the river network segments $s = (1, 3, 5, 9, 12, 16, 18, 22, 23)$ as shown in Figure 6, are compared in Figure 12. This comparison includes inferences made using WSE data from nadir altimetry and gauges, as well as from SWOT data alone.

Both assimilation experiments "N4l.2019" and "SWOT.CalVal," result in the inference of spatially distributed bathymetry-friction over the network, along with corrections to upstream inflows. It is important to recall that those estimations are performed from different priors, either $\boldsymbol{\theta}^{(0)}_{N4l}$ or $\boldsymbol{\theta}^{(0)}_{SWOT}$, based on the median discharge used to infer prior bathymetry as explained before. Moreover, both experiments are performed with identical setup for covariance matrices, for weights $\sigma_{\square}$ and correlation length $L_{\square}$.

The inferred parameters of the hydraulic model represent optimal solutions of the inverse problem (Equation 9) given the WSE data considered. These parameters effectively describe the bathymetry, friction and inflows that achieve the best fit to the WSE data used.

The calibrated hydraulic models obtained can be utilized to derive stage-fall-discharge laws for operational discharge forecasting using SWOT WSE and WS slopes (cf. Malou et al. (2021)). Aditionnally, a network scale hydrological-hydraulic approach is relevant for upgrading SWOT discharge products, and will be used in future research on HiVDI Larnier et al. (2020). These upgrades would benefit from better constraints on the double regionalization problem, which involves estimating uncertain or unknown spatio-temporal hydrological and hydraulic parameters from sparse data.

All assimilation experiments, using the same channel width data W^*, result in the inferrence of non-trivial channel HCs (cf. definition in Montazem et al. (2019)). These controls are depicted in Figure 12 and in the flow profiles by segment in Appendix G. The inferred controls enable the production of more realistic WS signatures with respect to the assimilated WSE data, in the sense of the observation cost function. Notably, More spatial variations are obtained in the bathymetry inferred with the denser SWOT data.

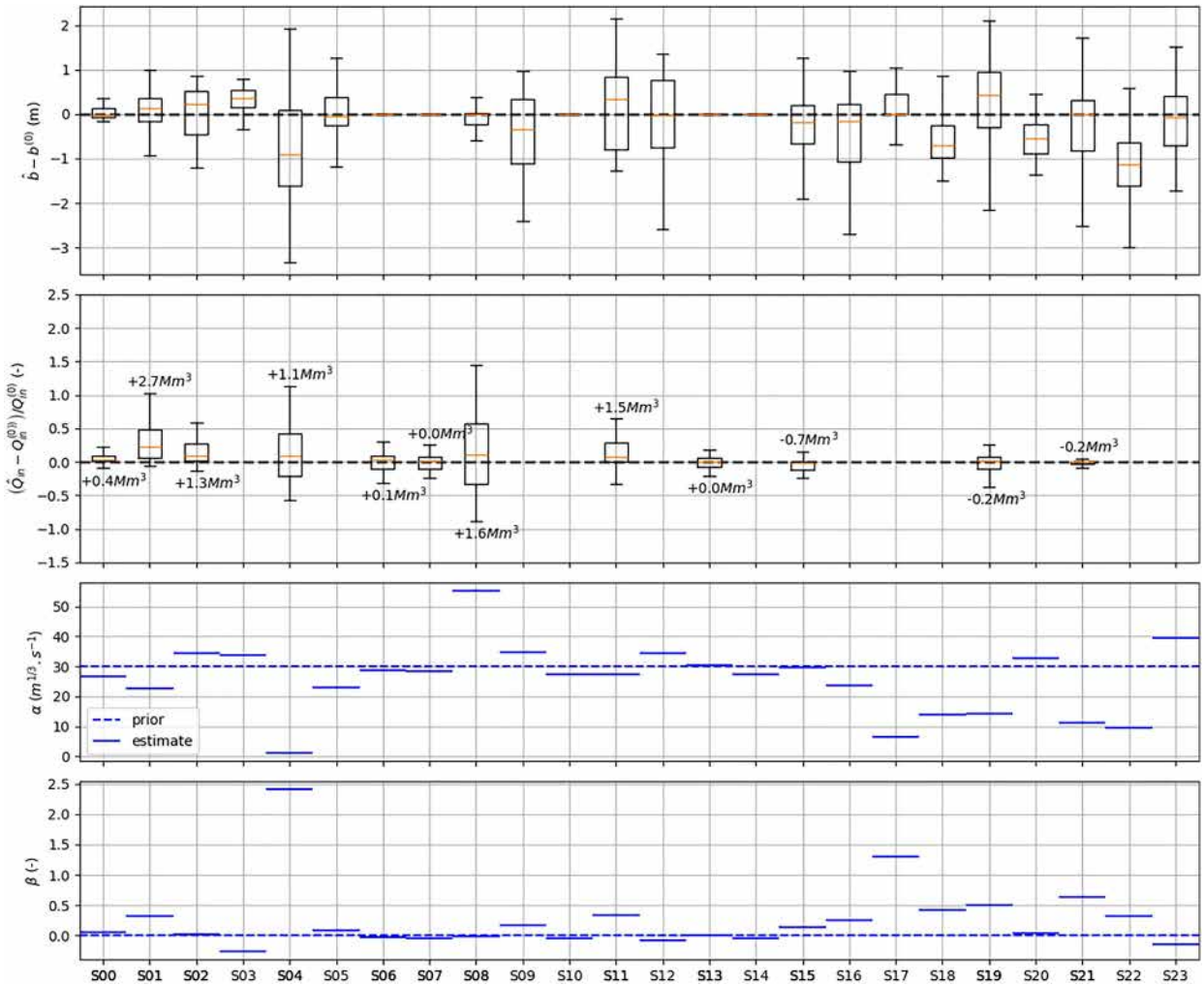

Figure 11. Relative correction of hydraulic model parameters after assimilation of SWOT water surface elevation data in the experiment "SWOT.CalVal." The figure shows inferred parameters $\hat{\boldsymbol{\theta}}$ by variational data assimilation from the background $\boldsymbol{\theta}^{(0)}_{SWOT}$, represented by segment of the river network "S00" to "S23": boxplots of spatially distributed corrections (top) of bathymetry $b(s,x)$ at $N_b = 2572$ hydraulic cross sections and of (second) inflow discharge hydrographs $Q^{t=1..T_u}_{in,u=1..N_{BC}}$ at $N_{BC} = 12$ inflows,(third and fourth) friction parameters $\hat{\alpha}$ and $\hat{\beta}$ over the 24 segments composing the simulated river network.

Regarding inflow correction, this study only considered upstream inflows, which correspond to 36% of the basin drainage area. The inference of the remaining numerous lateral inflows, which vary in magnitude depending on their corresponding drainage area and forcing, is a challenging issue (cf. Pujol et al. (2020) for an analysis of frequential identifiability of inflows, see also Brisset et al. (2018)). This aspect should be addressed in further research.

The transposability of the hydraulic parameters obtained with the VDA approach would be feasible and coherent if they were calibrated simultaneously with hydrological model parameters. This simultaneous calibration could be used for temporal extrapolation. More generally, this pertains to the difficult issue of joint optimization of spatio-temporally distributed parameters of a H&H model.

Such an approach would be feasible with the present VDA method applied to a differentiable H&H solver as proposed in Pujol et al. (2022). Additionally, these approaches would benefit from differentiable regionalization schemes included into the forward model to map physical descriptors onto model parameters. This has been demonstrated with a regionalization neural network in Huynh et al. (2023) or even with a learnable spatially distributed hydrological model on top of a differentiable hydraulic model (Huynh et al., 2024). These elements are

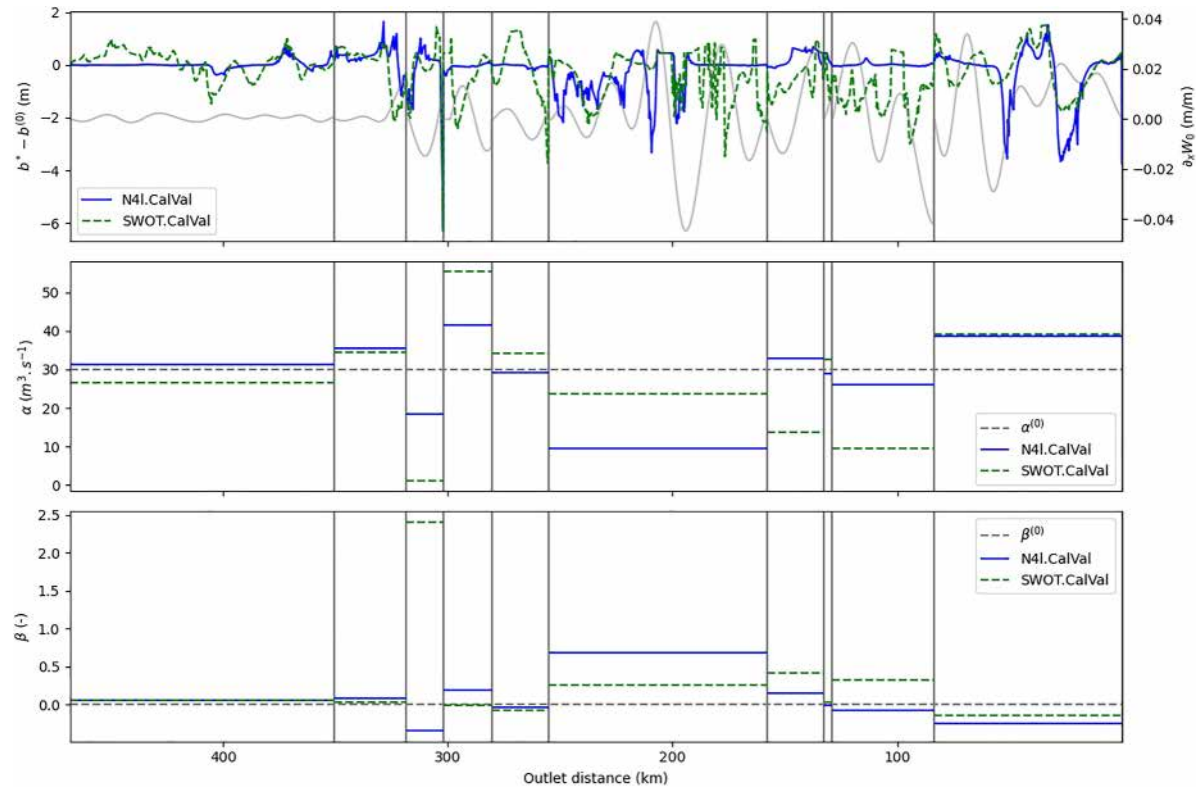

Figure 12. Longitudinal profiles along the Maroni main stream, segments $s = (1, 3, 5, 9, 12, 16, 18, 22, 23)$, of calibrated parameters after VDA: bathymetry $\hat{b}$ and friction coefficients α and β, along with channel width gradient $\partial_x W_0$ (gray line), for the "N4I.CalVal" experiment (blue) and "SWOT.CalVal" experiment (dashed green).

key components of a learnable, basin-scale physical model that can effectively integrate satellite hydraulic visibility.

5. Conclusion

This article presents a novel study on enhancing river network scale hydrological-hydraulic (H&H) models, by leveraging the unprecedented hydraulic visibility from the recently launched SWOT satellite. This is complemented by altimetry and imagery from other state-of-the-art satellites used to build the prior model geometry. A processing chain is proposed for the construction of a consistent prior hydraulic model geometry using multi-satellite data, including accurate images for dynamic water extents and a hydrological model. This work presents, for the first time to our best knowledge, a VDA process over a river network hydraulic model fed by a semi-distributed hydrological model, in a poorly gauged basin. Based on the obtained results and from the performed analysis, the following conclusions can be drawn:

- The proposed variational approach represents a powerful optimization and diagnostic tool for differentiable H&H models and spatio-temporal parameters estimation problems using multi-source data. The gradient values $\nabla_{\boldsymbol{\theta}} j(\boldsymbol{\theta})$, enable to analyze spatially distributed sensitivity maps of simulated quantities (with respect to some parameters present in the parameter vector $\boldsymbol{\theta}$). Moreover, such gradient maps can be used to estimate Sobol total sensitivity indices following the derivative-based sensitivity measure methodology introduced in Sobol' and Kucherenko (2009), and applied using numerical adjoint models for example, in lumped hydrology in Chelil et al. (2022) or in 2D hydraulic modeling in Pujol et al. (2024).
- This study addresses the challenge of closing the ill-posed inverse problem of inferring river discharge from WS measurements alone, see Larnier et al. (2020). The method builds upon the HiVDI algorithm (Larnier et al., 2020; Larnier & Monnier, 2023) focusing on single river portions, but achieves closure of the ill-posed problem through the physical enrichment provided by sequentially coupling a hydrological model with the hydraulic model over a complete river network. This approach uses the same computational tools and

ingredients but leverages richer physical information and data sets at basin scale, enabling the closure of the problem.

This approach is applicable to other basins worldwide, utilizing open-source remote sensing data, for instance. This work opens up avenues for further research. Immediate to mid-term work perspectives include the following:

- Assimilation of SWOT science orbit data, which is sparser in time but provides nearly full spatial coverage at basin scale, both alone and in combination with other data available. This approach aims to investigate their informative power and address frequential inferrability issues in detail, also considering large number of lateral inflows in function of available data.
- Application of the approach to gauged basins, utilizing massive data sets that include in situ measurements, drone data, and satellite observations.
- Studying how to improve SWOT discharge product using integrated basin scale H&H network models.
- Advanced data-model error accounting within Bayesian framework.
- Fully differentiable hydrological-hydraulic models (Pujol et al., 2022), incorporating learnable parts (Huynh et al., 2023), to enable simultaneous optimization of hydrological and hydraulic parameters from SWOT and other data. Such approaches offer a offer a promising pathway to address the double H&H regionalization problem, where data are typically sparser than model parameters and rarely fully informative or constraining. For instance, even a lumped conceptual hydrological model faces equifinality issues when calibrated from a discharge time series.

The computational software used in this work is open source DassFlow (2023) The computation kernel written in Fortran is wrapped in Python. This architecture supports integration with various libraries for signal processing, geographical treatments and machine learning, facilitating the development of hybrid deterministic-ML methods in its VDA framework (for large-scale parameter identification or calibration).

Appendix A: H&H Model and Numerical Resolution

A semi-distributed hydrological model $\mathcal{M}_{rr}$ provides spatio-temporal discharges estimates $Q_{rr}(x',t),\ \forall\ tx' \in \Omega_{rr},\ \forall\ tt \in [0,T]$. These estimates are used to inflow the hydraulic model at N_{in} inflow points, including upstream BCs and lateral inflows, at the border of the hydraulic domain Ω_{hy}.

The Saint-Venant equations are solved on each segment of the river network, and the continuity of the flow between segments is ensured by applying an equality constraint on water levels and mass conservation at the confluence between two segments.

BC_S are classically imposed (subcritical flows here) at boundary nodes (main hydrological inflows here) with inflow discharges $Q_{in,i=1..N_{BC}}(t)$ at N_{BC} upstream nodes and WSE $Z_{avl}(t)$ at the downstream node; lateral hydrographs $q_{lat,i=1..N_{lat}}(t)$ at N_{lat} lateral inflow nodes (such that $N_{in} = N_{BC} + N_{lat}$). The initial condition is set as the steady state backwater curve profile $Z_0(x) = Z\big(Q_{in}(t_0), q_{lat,1..L}(t_0)\big)$ for hot-start. This 1D Saint-Venant model is discretized using the classical implicit Preissmann scheme (see e.g., Cunge et al. (1980); Roux (2004)) on a regular grid of spacing Δx using a double sweep method to handle flow regimes changes. An hourly time step Δt is used. This model is implemented into the computational software DassFlow1D. For more details see DassFlow documentation (https://dasshydro.github.io/doc/); accurate finite volume scheme are also available; source code on GitHub (https://github.com/DassHydro/dassflow1d).

Appendix B: Observation Data Set

We denote by $\boldsymbol{Y}^*$ the set of multi-source observations of hydraulic responses over the river network domain Ω_{hy}, which we aim to integrate into the flow model. This set includes in altimetric WSE and flow top width, which are unevenly spaced but cover the entire spatial domain densely. These observations come from various sources such as imagery, drifting or wide swath altimetry, in addition to multi-mission nadir altimetry.

In the general case, a multi-satellite data set, composed of WS elevation and width observations, can be written as:

$$\boldsymbol{Y}^* := \left\{\left(Z^*\left((s,x)_{vs=1..N_z}, t_{pz=1..P_z(oz)}\right); W^*\left((s,x)_{ws=1..N_w}, t_{pw=1..P_w(ow)}\right)\right\} \tag{B1}$$

with $(s,x)_{\square}$ denoting the spatial location of WSE or WSW measurements sorted in ascending, and $t_{\square}$ representing the observation times at these location. N_z and N_w represent the number of WSE and WSW observation points accross the river network domain Ω_{hy}, respectively. N_{oz} and N_{ow} represent the number of observation times for each WSE measurement location $x_{oz=1..N_z}$ and WSW location $x_{ow=1..N_w}$ respectively. Similarly, $t_{\square}$ denotes measurements times.

In the case of SWOT, Z and W measurements are synchronous in time and space, and the data set simplifies to:

$$\boldsymbol{Y}^* := (Z^*, W^*)\,(x_{o=1..N_o}, t_{p=1..p(o)}) \tag{B2}$$

In this work, SWOT data are not used for geometry parameterization but only in assimilation. WS width are determined from dynamic water masks are extracted from Sentinel radar data. This enables the definition of XSs geometries.

Appendix C: Regularization for the Variational Data Assimilation Algorithm

The VDA algorithm is those developed in the HiVDI algorithm, see DassFlow (2023); Larnier and Monnier (2023); Larnier et al. (2020). The VDA formulation is based on covariance operators and the following change of control variable (see e.g. Haben et al. (2011); Larnier et al. (2020)): $k = B^{-1/2}\left(\boldsymbol{\theta} - \boldsymbol{\theta}^{(0)}\right)$.

The background $\boldsymbol{\theta}^{(0)}$ (first guess, or prior in statistics) on the sought parameter from which optimization is started, and the background error covariance matrix B, both depend on the information available and a priori physical knowledge of the system and of the unknowns. With this change of control variable we are interested in the minimization of the following cost function: $j(\boldsymbol{k}) = \frac{1}{2}\left\| \mathcal{M}\left(\boldsymbol{\theta}^{(0)} + B^{1/2}\boldsymbol{k}\right) - Y^* \right\|_O^2$.

The choice of B is crucial for the optimization and influences the inferred solution.

Assuming uncorrelated unknowns, the matrix B is block diagonal: $B = \mathrm{diag}\left(B_Q, B_b, B_K\right)$. each block $B_{\square}$ being defined from the decreasing exponential kernels following Malou and Monnier (2022):

$$\left(B_Q\right)_{i,j} = \left(\sigma_Q\right)^2 \exp\left(-\frac{|t_j - t_i|}{L_Q}\right);\ \textit{and}\ \ \left(B_b\right)_{i,j} = \left(\sigma_b\right)^2 \exp\left(-\frac{|x_j - x_i|}{L_b}\right);\ \textit{and}\ \ B_K = \mathrm{diag}\left(\sigma_\alpha^2, \sigma_\beta^2\right) \tag{C1}$$

with L_Q and L_b acting as correlation scales defined a priori from empirical physical knowledge. The scalar values $\sigma_{\square}$ define the weighting effect in parameters optimization.

Appendix D: Processing Algorithm for ICESat-2 ATL13 Data to Extract WSE

ATL13 data is positionned along 6 beams (organized by pairs gt1r/gt1l, gt2r/gt2l, gt3r/gt3l) and presented as a set of beam-points (referenced by their longitude and latitude) above inland water bodies such as rivers and lakes only. Our goal is to aggregate this data to build WSE timeseries at VS over the Maroni river. For this purpose, we need a set a line geometry representing the river network centerline and a polygon geometry delineating the a priori watermask where ATL13 data will be extracted and processed.

D1. Delineating the Study Domain Watermask

The watermask is taken from the Pekel's global Surface Water Data set, considering water pixels with an occurrence of at least 50%. This is an adequate hypothesis given the relatively low variability of top width found on the Maroni. This was confirmed by analyzing Sentinel 1-derived WSW of dynamic water masks obtained with ExtractEO chain.

For the studied Maroni basin, we considered and applied the following steps:

1. Polygonize Pekel watermask,
2. Application of a buffer with distance 0.0003° (as Pekel mask resolution is of 0.00025°): buffer function extends the boundaries of a given geometry and rounds its egde by the input distance.

3. Manual correction to fill missing river branches based on expert knowledge. Also, it was chosen to fully include under the watermask braided zone without distinguishing the individual river branches.
4. Cascaded union to merge individual polygons that intersect together.
5. Small tributaries not represented by the Pekel product are added by building a polygon from a buffer around the riverline of those small tributaries and merging them to the rest of the domain (for the Maroni domain only).

D2. WSE Data Extraction

ICESat-2 products are organized by granule containing data below a full orbit, each orbit being divided in 6 beams (gt1l/gt1r/gt2l/gt2r/gt3l/gt3r). A individual ICESat-2 is a beam point caracterized by its coordinates (lon, lat) and an elevation wse (above the WGS84 ellipsoid). ICESat-2 have to be extracted and aggregated under virtual stations to derive elevation timeseries and XSs for the effective hydraulic model.

For each granule, the following processing is applied:

1. Extraction of all beam points within the study domain polygon.
2. Each beam point is "projected" along the river centerline. From this linear referencing, a curvilinear abscissa x_s [m] (distance along the centerline from the upstream edge) and a distance-to-the-river d_r [m] (distance between the original beam point and its projection) are associated to each beam point.
3. Then, each beam point is associated to the closest VS according to their x_s. A distance d_s ($=x_{s,VS} - x_s$) and an angle ($=\arctan \frac{d_r}{d_s}$) are derived accordingly.
4. Once all beam points are extracted, potential outliers have to be detected and flagged out for further processing (see Appendix D3).
5. For each VS, time-aggregation is easily done by gathering beam points that comes from the same granule and the same cycle.
6. subsequently, beam points gathered in the same time index are spatially-aggregated into a single elevation measurements (see Appendix D3).

D3. More Details on the Processing of ATL13 Data

D3.1. Outlier Detection

Each river segment is divided into sub-segments of 5 km. Over each sub-segment, monthly subset of beam points which x_s fall on this sub-segment, are inspected. A linear regression of the elevation with respect to x_s from the ICESat-2 beam points subset is estimated with the standard deviation σ of the gap between the measured elevation and the corresponding (with respect to x_s) elevation from the linear regression. All points that are above 3σ are flagged out as outliers.

D3.2. Space Aggregation

D3.2.1. Version 1

Every beam point attributes (i.e. wse, lon, lat, x_s, d_s, d_r, angle, dt as seconds from 1 January 2028) are simply averaged with a classical mean.

D3.2.2. Version 2

Weighted averaged where each beam point weight w is defined by

$$w = 1. - \left\| \frac{d_s}{d_{s_max}} \right\|.$$

D3.2.3. Draw XSs

For each segment and its associated subdomain polygon

1. The domain polygon is split into voronoi regions centered around the virtual stations of the polygon. Each region delineates any beam point which the closest VS is the region's associated VS.
2. The XSs is draw following the constraint below:
   - The section is contained within the associated voronoi region
   - The section contains the VS
   - The section should cross the river with an angle close to normal to the river centerline
   - The section have to cross any region boundaries that are common with the overall polygon exterior boundaries

If one can not draw a XS that respects the constraints above, a section normal to the river centerline is drawn with a width equal to the largest d_r.

Appendix E: Processing of Watermasks Images to Extract River Width

River widths were extracted from a collection of 121 watermasks computed using the ExtractEO algorithm (Maxant et al. (2022)) on available Sentinel 1 images for the period 2021-01-01–2022-12-31. The river widths were computed using the dedicated BAS algorithm (https://github.com/CS-SI/BAS). The methodology is fully applicable on other zone of interest, even with watermask computed from other water classification algorithm (provided as binary classification where water is 1 and land, etc., is 0).

These widths are usable for non rectangular XS parameterization but a simple rectangular XS is sufficient for this study on the Maroni River. More complex XSs have been used on the Niger basin, leading to a model setupthat enables good realism. However, this is not presented here and left for further research. Note that the vertical referencing of these dynamic water extents over time can be performed with altimetric measurements around image acquisition date while simultaneous WSE and WSW measurement are obtained with SWOT.

Appendix F: SWOT L2 Wavelet Based Filtering and Segmentation Algorithm

The wavelet-based filtering and segmentation algorithm is designed to process WSE longitudinal profiles, such as those provided by SWOT or by in situ GNSS, while preserving the WS signatures of HCs. This algorithm is based on the approach and MATLAB codes of Montazem et al. (2019). The idea is to use wavelet processing to isolate the signatures of local HCs, as hydraulic variability manifests at multiple spatial scales. Using a wavelet basis allows for the decomposition of free surface spatial profiles with high accuracy while retaining localized frequency information. A unique feature of this approach is the use of wavelets to both denoising and segmenting (not used here) signals in a consistent, space-frequency localized manner. This method introduces minial oscillations into the reconstructed filtered signal and is well suited for unsteady signals and detecting strong curvature signals. This algorithm, called pyrscwt (Python River Segmentation with Continuous Wavelet Transform), is based on a custom Python implementation of a continuous wavelet transform, enabling accurate 1D signal projections and reconstructions.

The proposed algorithm aims to (a) efficiently denoise L2 SWOT-type river node-scale data (RiverObs product at spatial resolution $dx \sim 200$ m), (b) perform a segmentation of a river portion into reaches, at user defined scale, that best preserves hydraulic signals and ultimately contributes to the quality of flow modeling and its coherence with multi-mission altimetry data. In the present article only denoising of SWOT RiverObs WSE $Z(x)$ data is performed with pyrscwt before their assimilation into the hydraulic model at local XS scale.

The proposed algorithm taking as input a spatial signal of WSE $Z(x)$ signals, sampled at a constant spatial step, consists in the following steps:

- Signal resampling and symetrization (prolongation of the signal on its spatial borders).
- Automated choice of the wavelet projection basis (7 mother wavelets and 10 orders for each) such that the reconstruction error $\epsilon_{\hat{Z}}$ is minimal.
- Filtering and segmentation of the original signal $Z(x)$ obtained by a low-pass filtering of wavelet coefficients corresponding to spatial variations below a user defined cutoff length scale λ_c. An additional physical criterion is used to filter wavelet coefficients: at the scale of measurements a counter slope in the WS is unphysical, that is $\partial_x Z > 0$. For a zone of length l_d with a counter slope we consider a centered window of length $3l_d$, since we

do not know whether this unphysical counterslope stems from over-understimations upstream or downstream, on which wavelet coefficients are iteratively filtered until $\partial_x \hat{Z} \leq 0$.

- HC sections (HCs) detection with the reconstructed signal $\hat{Z}(x)$ that is "error free" via maximum of WS curvature $\partial_x^2 \hat{Z}(x)$.

Appendix G: Detail on Inferred Parameters

Figure G1.

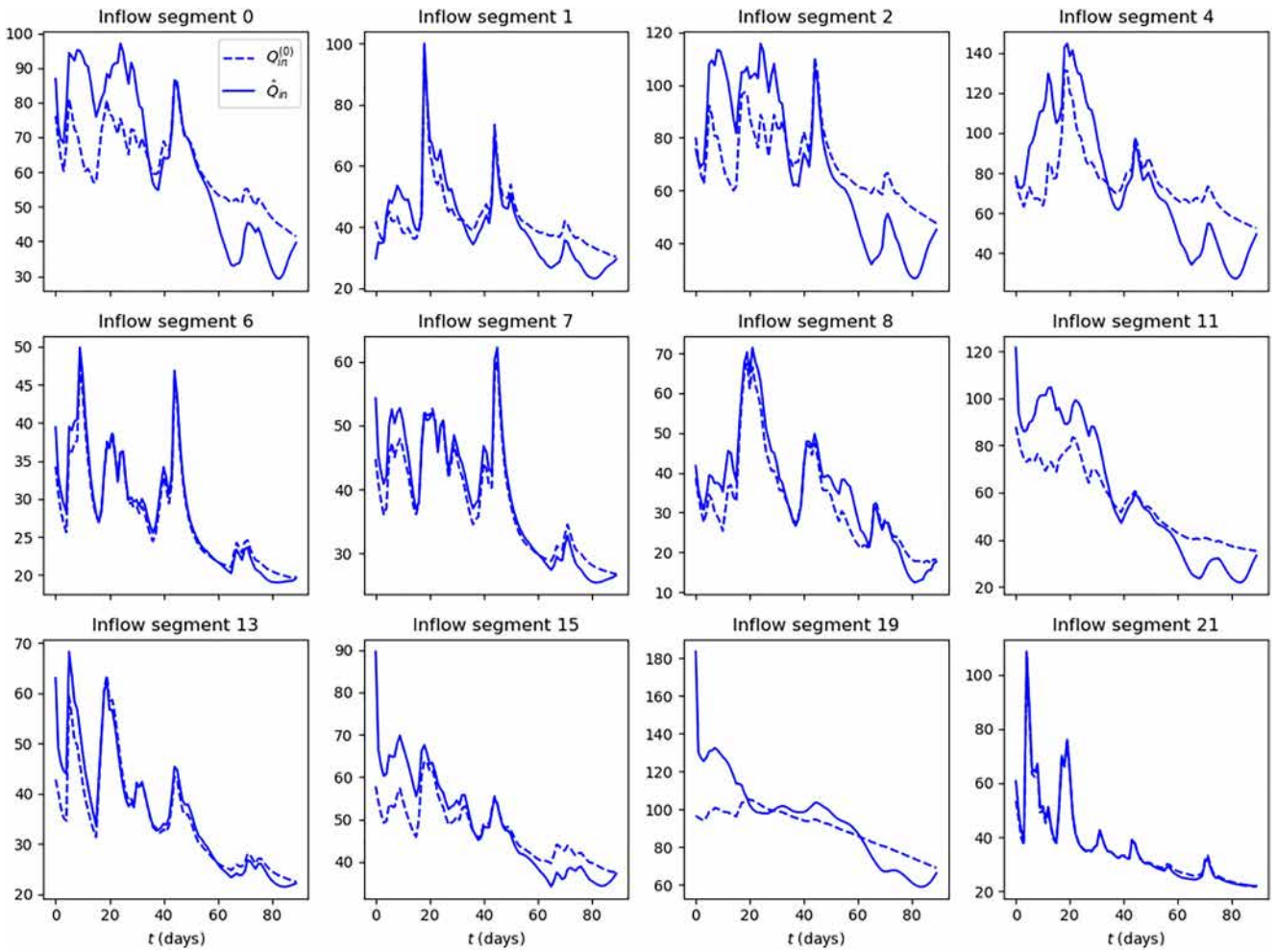

Figure G1. Inferred inflow hydrographs N4l.2019.

Figure G2.

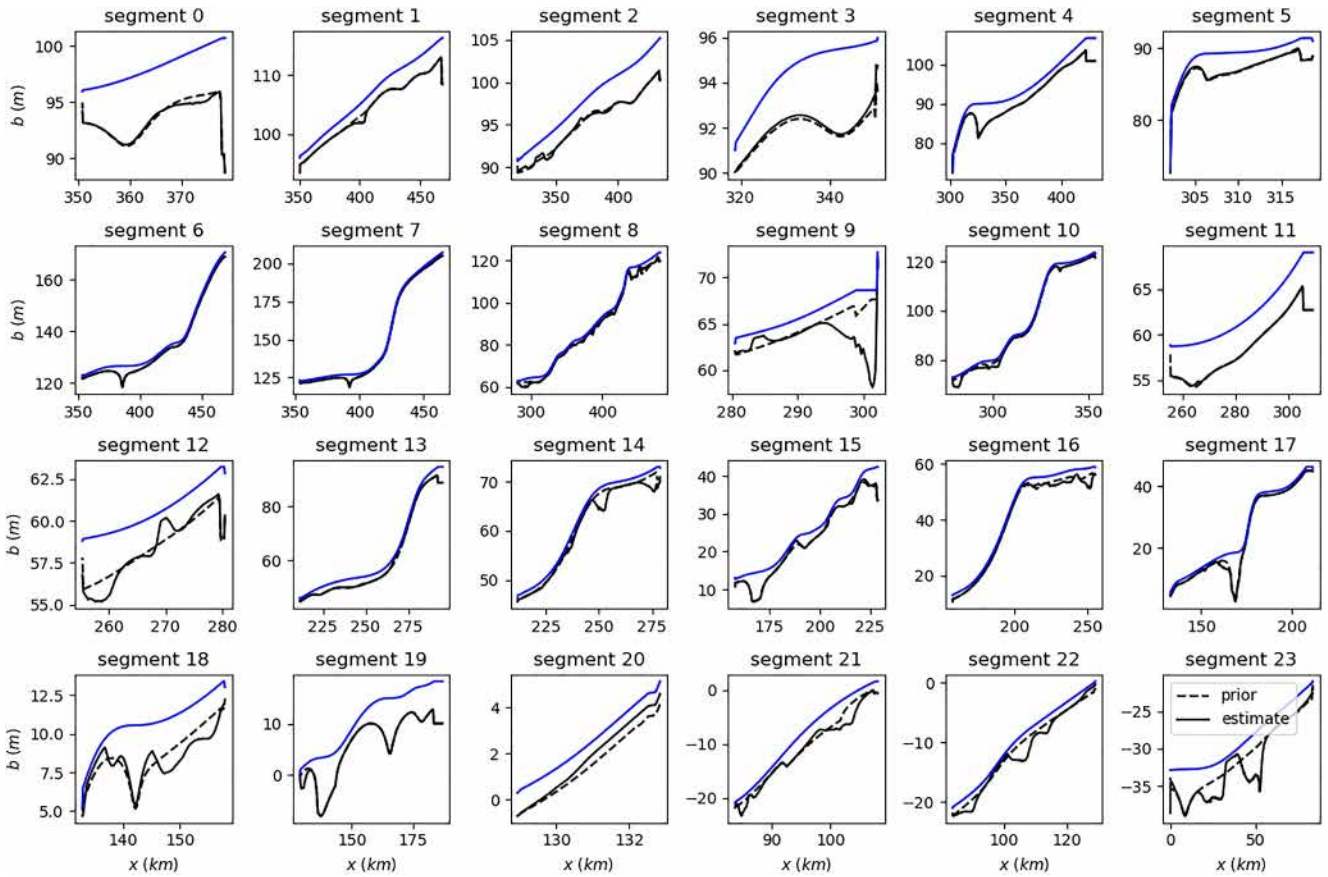

Figure G2. Inferred bathymetry N4l.2019.

Figure G3.

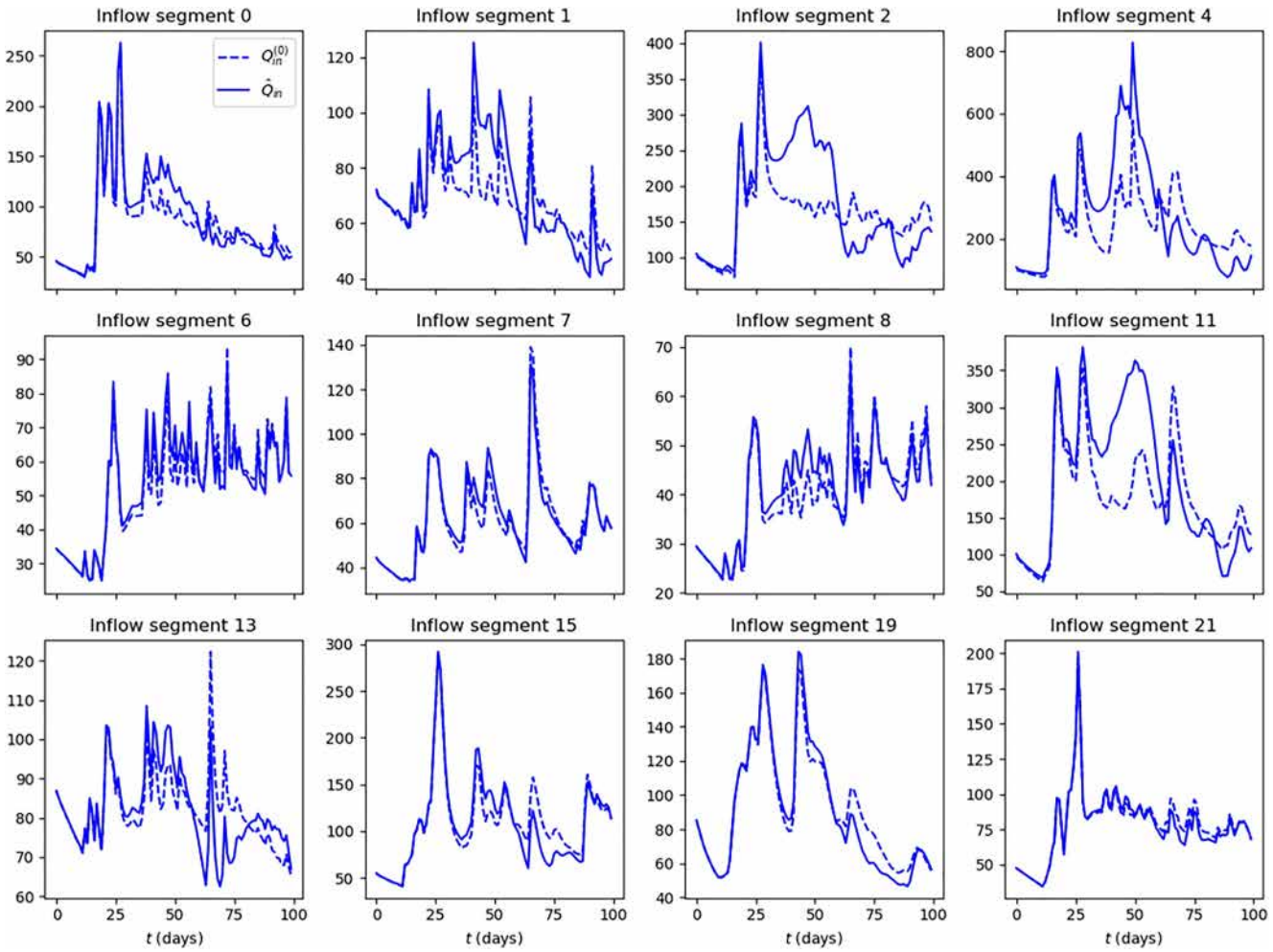

Figure G3. Inferred inflow hydrographs N4l.CalVal.

Figure G4.

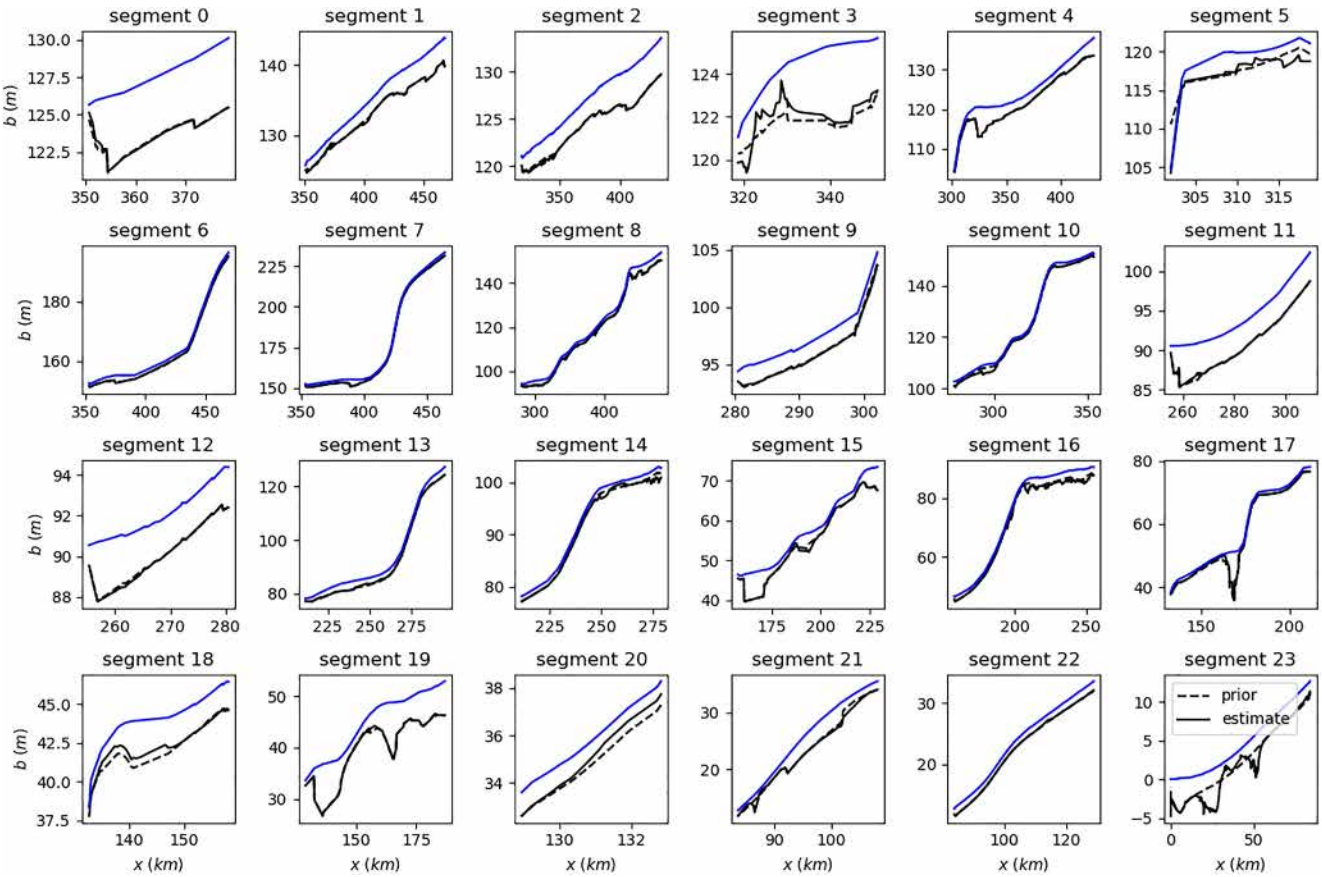

Figure G4. Inferred bathymetry N4l.CalVal.

Figure G5.

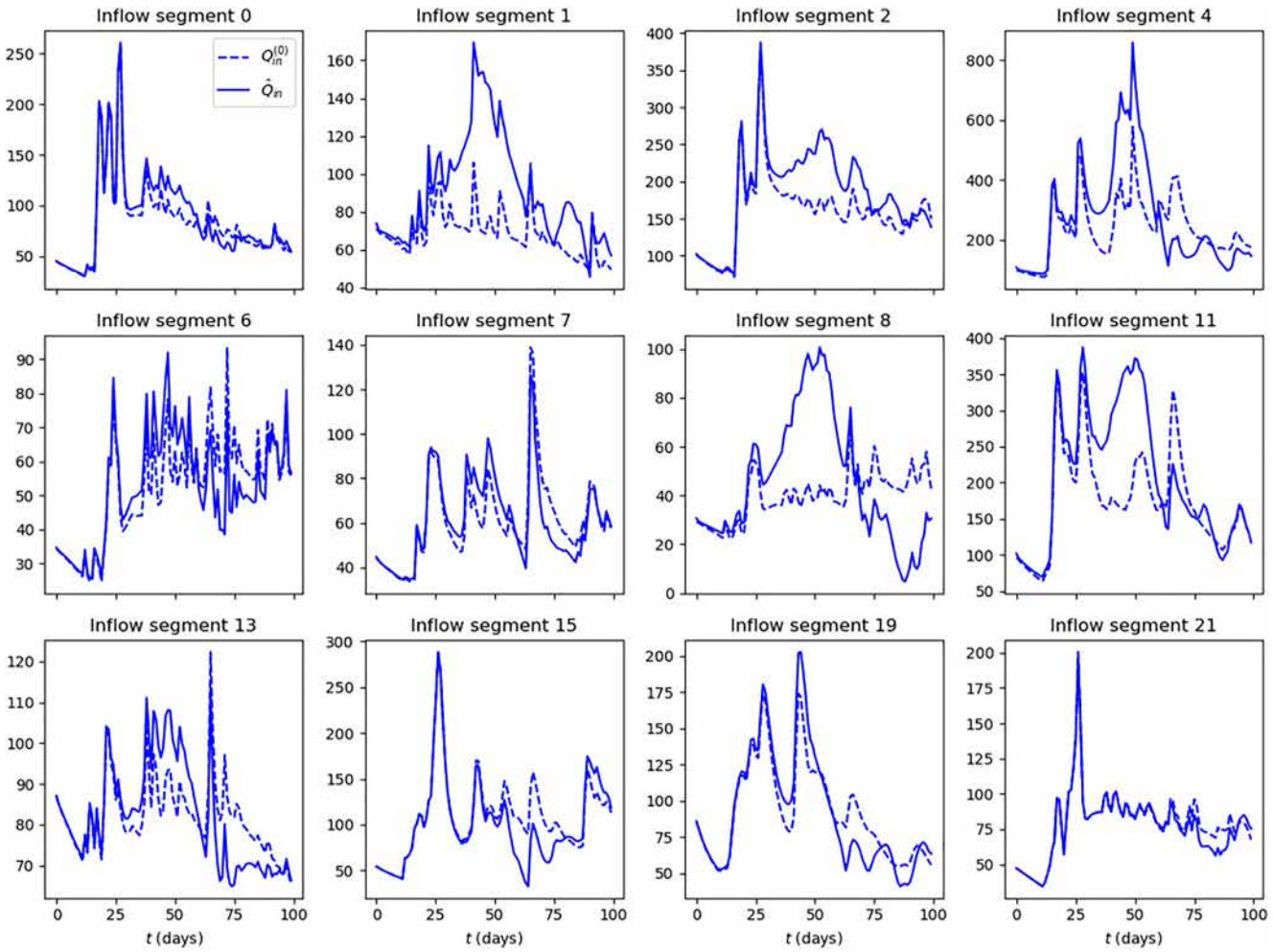

Figure G5. Inferred inflow hydrographs SWOT.CalVal.

Figure G6.

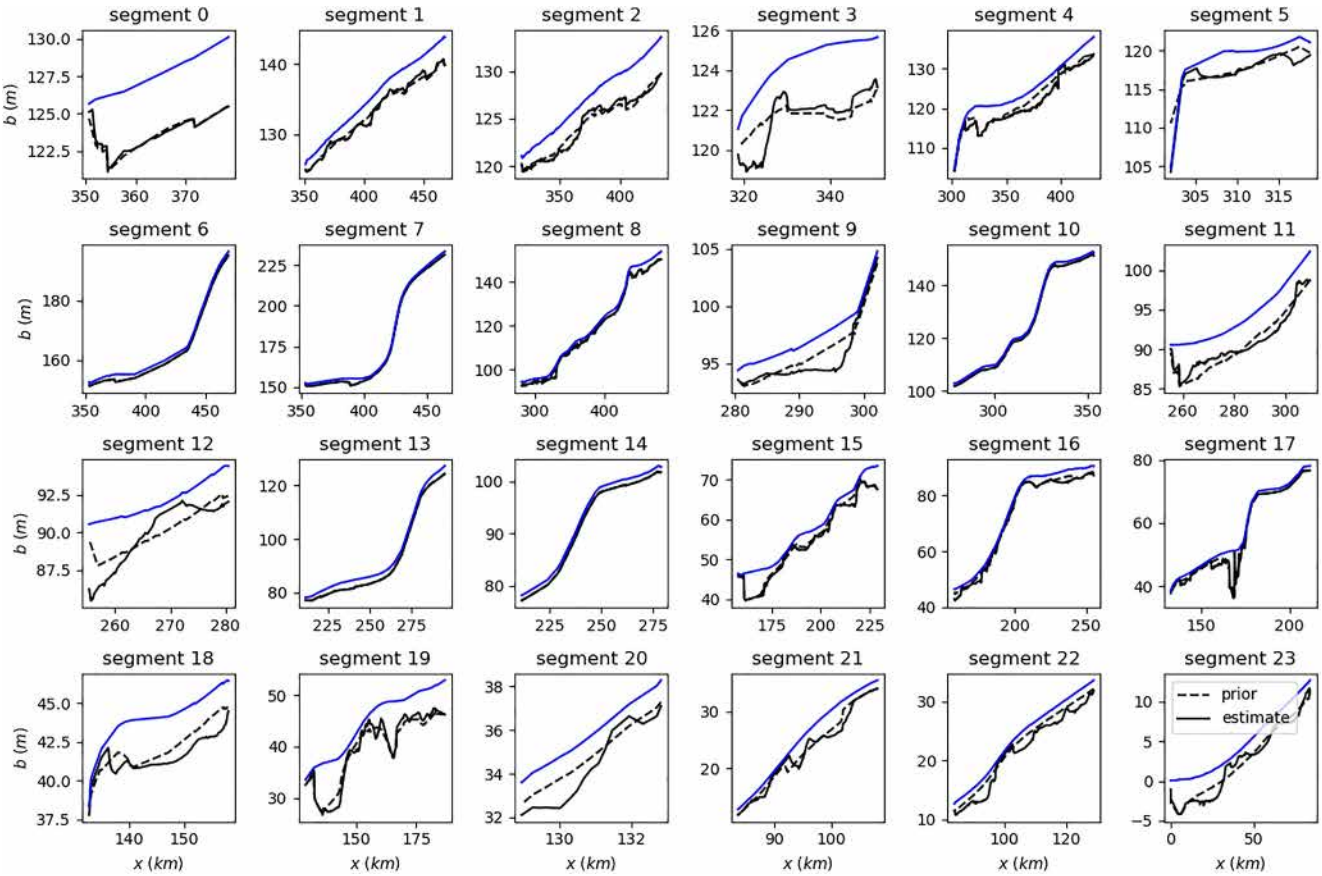

Figure G6. Inferred bathymetry SWOT.CalVal.

Figure G7.

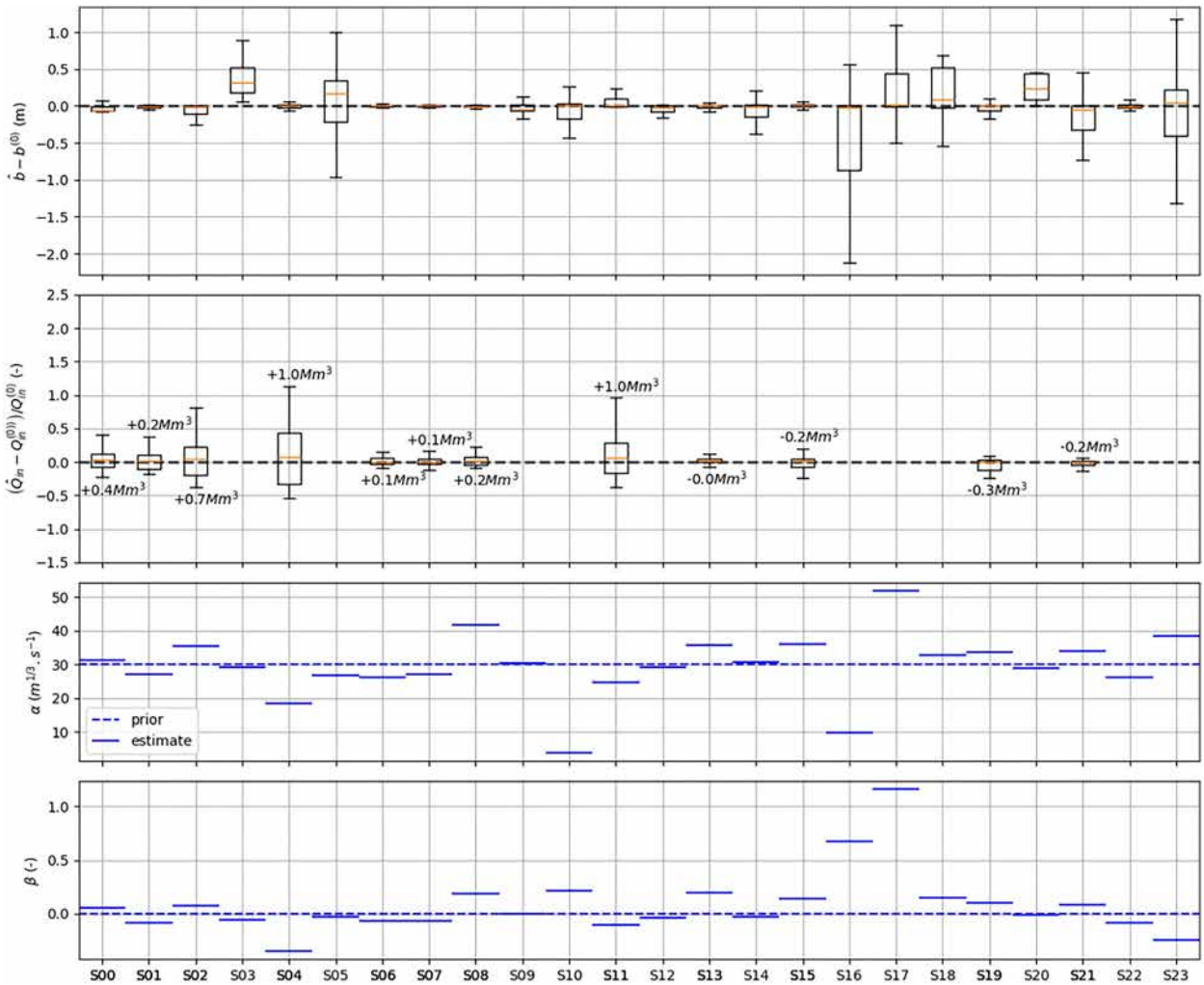

Figure G7. Model parameters $\hat{\theta}$ inferred by variational data assimilation in the N4l.CalVal experiment.

Data Availability Statement

This article is based on open source data, data set is accessible here: https://doi.org/10.5281/zenodo.15673811. DassFlow source code is open source and available at https://github.com/DassHydro/dassflow1d. MGB is also an open source code and available at https://www.ufrgs.br/lsh/mgb/downloads/mgb-4-5-new-documentation/.

Acknowledgments
CNES for financial support of several authors, and also for engineering support regarding processing of WSW data and SWOT data. DEAL Guyane for processing discharge data. Evanne Angenent for data processing and contribution to the first modeling of the Maroni basin with MGB-DassFlow1D, during an internship at INRAE and DEAL Cayenne. Joao Hemptinne for participation to re-implementation of the segmentation algorihtm.

References

Altenau, E. H., Pavelsky, T. M., Durand, M. T., Yang, X., Frasson, R. P. d. M., & Bendezu, L. (2021). The surface water and ocean topography (SWOT) mission river database (sword): A global river network for satellite data products. *Water Resources Research*, *57*(7), e2021WR030054. https://doi.org/10.1029/2021WR030054

Andreadis, K. M., Brinkerhoff, C. B., & Gleason, C. J. (2020). Constraining the assimilation of SWOT observations with hydraulic geometry relations. *Water Resources Research*, *56*(5), e2019WR026611. https://doi.org/10.1029/2019WR026611

Asch, M., Bocquet, M., & Nodet, M. (2016). *Data assimilation: Methods, algorithms, and applications* (Vol. 11). SIAM.

Bonnans, J. F., Gilbert, J. C., Lemaréchal, C., & Sagastizábal, C. A. (2006). *Numerical optimization: Theoretical and practical aspects*. Springer. Retrieved from https://www.springer.com/gp/book/9783540354453

Brisset, P., Monnier, J., Garambois, P.-A., & Roux, H. (2018). On the assimilation of altimetric data in 1D Saint-Venant River flow models. *Advances in Water Resources*, *119*, 41–59. https://doi.org/10.1016/j.advwatres.2018.06.004

Chelil, S., Oubanas, H., Henine, H., Gejadze, I., Malaterre, P. O., & Tournebize, J. (2022). Variational data assimilation to improve subsurface drainage model parameters. *Journal of Hydrology*, *610*, 128006. https://doi.org/10.1016/j.jhydrol.2022.128006

Chow, V. (1959). *Open-channel hydraulics*. Mc Graw-Hill.

Collischon, W., Allasia, D., Da Silva, B., & Tucci, C. E. M. (2007). The MGP-IPH model for large-scale rainfall—runoff modelling. *Hydrological Sciences Journal*, *52*(5), 878–895. https://doi.org/10.1623/hysj.52.5.878

Coppo Frias, M., Liu, S., Mo, X., Nielsen, K., Randall, H., Jiang, L., et al. (2022). River hydraulic modelling with Icesat-2 land and water surface elevation. *EGUsphere*, *2022*, 1–27. https://doi.org/10.5194/egusphere-2022-377

Cunge, J. A., Holly, M. F., & Verwey, A. (1980). *Practical aspects of computational river hydraulics*. Pitam Publishing.

DassFlow. (2023). Data assimilation for free surface flows. Open source computational code. Retrieved from https://github.com/DassHydro

de Paiva, R. C. D., Buarque, D. C., Collischonn, W., Bonnet, M.-P., Frappart, F., Calmant, S., & Bulhões Mendes, C. A. (2013a). Large-scale hydrologic and hydrodynamic modeling of the Amazon river basin. *Water Resources Research*, *49*(3), 1226–1243. https://doi.org/10.1002/wrcr.20067

Dingman, S. (2009). *Fluvial hydraulics*. Oxford University Press.

Dingman, S. L. (2007). Analytical derivation of at-a-station hydraulic–geometry relations. *Journal of Hydrology*, *334*(1), 17–27. https://doi.org/10.1016/j.jhydrol.2006.09.021

Dingman, S. L., & Afshari, S. (2018). Field verification of analytical at-a-station hydraulic-geometry relations. *Journal of Hydrology*, *564*, 859–872. https://doi.org/10.1016/j.jhydrol.2018.07.020

Durand, M., Gleason, C. J., Pavelsky, T. M., Prata de Moraes Frasson, R., Turmon, M., David, C. H., et al. (2023). A framework for estimating global river discharge from the surface water and ocean topography satellite mission. *Water Resources Research*, *59*(4), e2021WR031614. https://doi.org/10.1029/2021WR031614

Durand, M., Neal, J., Rodríguez, E., Andreadis, K., Smith, L., & Yoon, Y. (2014). Estimating reach-averaged discharge for the river Severn from measurements of river water surface elevation and slope. *Journal of Hydrology*, *511*, 92–104. https://doi.org/10.1016/j.jhydrol.2013.12.050

Eggleston, J., Mason, C., Bjerklie, D., Durand, M., Dudley, R., & Harlan, M. (2024). Siting considerations for satellite observation of river discharge. *Water Resources Research*, *60*(6), e2023WR034583. https://doi.org/10.1029/2023WR034583

Flipo, N., Mouhri, A., Labarthe, B., Biancamaria, S., Rivière, A., & Weill, P. (2014). Continental hydrosystem modelling: The concept of nested stream–aquifer interfaces. *Hydrology and Earth System Sciences*, *18*(8), 3121–3149. https://doi.org/10.5194/hess-18-3121-2014

Frasson, R. P. d. M., Durand, M. T., Larnier, K., Gleason, C., Andreadis, K. M., Hagemann, M., et al. (2021). Exploring the factors controlling the error characteristics of the surface water and ocean topography mission discharge estimates. *Water Resources Research*, *57*(6), e2020WR028519. https://doi.org/10.1029/2020WR028519

Garambois, P.-A., Calmant, S., Roux, H., Paris, A., Monnier, J., Finaud-Guyot, P., et al. (2017). Hydraulic visibility: Using satellite altimetry to parameterize a hydraulic model of an ungauged reach of a braided river. *Hydrological Processes*, *31*(4), 756–767. https://doi.org/10.1002/hyp.11033

Garambois, P.-A., Larnier, K., Monnier, J., Finaud-Guyot, P., Verley, J., Montazem, A.-S., & Calmant, S. (2020). Variational estimation of effective channel and ungauged anabranching river discharge from multi-satellite water heights of different spatial sparsity. *Journal of Hydrology*, *581*, 124409. https://doi.org/10.1016/j.jhydrol.2019.124409

Garambois, P.-A., & Monnier, J. (2015). Inference of effective river properties from remotely sensed observations of water surface. *Advances in Water Resources*, *79*, 103–120. https://doi.org/10.1016/j.advwatres.2015.02.007

Gejadze, I., & Malaterre, P.-O. (2017). Discharge estimation under uncertainty using variational methods with application to the full saint-venant hydraulic network model. *International Journal for Numerical Methods in Fluids*, *83*(5), 405–430. https://doi.org/10.1002/fld.4273

Gejadze, I., Malaterre, P.-O., Oubanas, H., & Shutyaev, V. (2022). A new robust discharge estimation method applied in the context of swot satellite data processing. *Journal of Hydrology*, *610*, 127909. https://doi.org/10.1016/j.jhydrol.2022.127909

Getirana, A. C. (2010). Integrating spatial altimetry data into the automatic calibration of hydrological models. *Journal of Hydrology*, *387*(3), 244–255. https://doi.org/10.1016/j.jhydrol.2010.04.013

Haben, S., Lawless, A., & Nichols, N. (2011). Conditioning of incremental variational data assimilation, with application to the met office system. *Tellus*, *63*(4), 782–792. https://doi.org/10.1111/j.1600-0870.2011.00527.x

Hascoet, L., & Pascual, V. (2013). The tapenade automatic differentiation tool: Principles, model, and specification. *ACM Transactions on Mathematical Software*, *39*(3), 1–43. https://doi.org/10.1145/2450153.2450158

Horner, I., Renard, B., Le Coz, J., Branger, F., McMillan, H. K., & Pierrefeu, G. (2018). Impact of stage measurement errors on streamflow uncertainty. *Water Resources Research*, *54*(3), 1952–1976. https://doi.org/10.1002/2017WR022039

Huynh, N. N. T., Garambois, P.-A., Colleoni, F., Renard, B., Roux, H., Demargne, J., & Javelle, P. (2023). Learning regionalization within a differentiable high-resolution hydrological model using accurate spatial cost gradients.

Huynh, N. N. T., Garambois, P.-A., Renard, B., Colleoni, F., Monnier, J., & Roux, H. (2024). Multiscale learnable physical modeling and data assimilation framework: Application to high-resolution regionalized hydrological simulation of flash floods. https://doi.org/10.22541/au.170709054.44271526/v1

Kubota, T., Aonashi, K., Ushio, T., Shige, S., Takayabu, Y. N., Kachi, M., et al. (2020). Global satellite mapping of precipitation (gsmap) products in the gpm era. *Satellite Precipitation Measurement*, *1*, 355–373. https://doi.org/10.1007/978-3-030-24568-9_20

Lague, D., & Feldmann, B. (2020). Chapter 2 - Topo-bathymetric airborne lidar for fluvial-geomorphology analysis. In P. Tarolli & S. M. Mudd (Eds.), *Remote sensing of geomorphology* (Vol. 23, pp. 25–54). Elsevier. https://doi.org/10.1016/B978-0-444-64177-9.00002-3

Larnier, K., & Monnier, J. (2023). Hybrid neural network–Variational data assimilation algorithm to infer river discharges from SWOT-like data. *Computers & Geosciences*, *27*(5), 853–877. https://doi.org/10.1007/s10596-023-10225-2

Larnier, K., Monnier, J., Garambois, P.-A., & Verley, J. (2020). River discharge and bathymetry estimation from SWOT altimetry measurements. *Inverse Problems in Science and Engineering*, *29*(6), 1–31. https://doi.org/10.1080/17415977.2020.1803858

Le Coz, J., Renard, B., Bonnifait, L., Branger, F., & Le Boursicaud, R. (2014). Combining hydraulic knowledge and uncertain Gaugings in the estimation of hydrometric rating curves: A Bayesian approach. *Journal of Hydrology*, *509*, 573–587. https://doi.org/10.1016/j.jhydrol.2013.11.016

Leopold, L., & Maddock, T. (1953). The hydraulic geometry of stream channels and some physiographic implications. *USGS Numbered Series*, *252*, 57pp. Retrieved from https://pubs.er.usgs.gov/publication/pp252

Malou, T., Garambois, P.-A., Paris, A., Monnier, J., & Larnier, K. (2021). Generation and analysis of stage-fall-discharge laws from coupled hydrological-hydraulic river network model integrating sparse multi-satellite data. *Journal of Hydrology*, *603*, 126993. https://doi.org/10.1016/j.jhydrol.2021.126993

Malou, T., & Monnier, J. (2022). Covariance kernels investigation from diffusive wave equations for data assimilation in hydrology. *Inverse Problems*. https://doi.org/10.1088/1361-6420/ac509d

Mansanarez, V., Le Coz, J., Renard, B., Lang, M., Pierrefeu, G., & Vauchel, P. (2016). Bayesian analysis of stage-fall-discharge rating curves and their uncertainties. *Water Resources Research*, *52*(9), 7424–7443. https://doi.org/10.1002/2016WR018916

Masson-Delmotte, V., Zhai, P., Pörtner, H.-O., Roberts, D., Skea, J., Shukla, P. R., et al. (2022). *Global warming of 1.5C: Ipcc special report on impacts of global warming of 1.5C above pre-industrial levels in context of strengthening response to climate change, sustainable development, and efforts to eradicate poverty*. Cambridge University Press.

Maxant, J., Braun, R., Caspard, M., & Clandillon, S. (2022). Extracteo, a pipeline for disaster extent mapping in the context of emergency management. *Remote Sensing*, *14*(20), 5253. https://doi.org/10.3390/rs14205253

Meyer Oliveira, A., Fleischmann, A., & Paiva, R. (2021). On the contribution of remote sensing-based calibration to model hydrological and hydraulic processes in tropical regions. *Journal of Hydrology*, *597*, 126184. https://doi.org/10.1016/j.jhydrol.2021.126184

Milly, P. (1994). Climate, interseasonal storage of soil water, and the annual water balance. *Advances in Water Resources*, *17*(1), 19–24. https://doi.org/10.1016/0309-1708(94)90020-5

Monnier, J. (2021). Data assimilation, optimal control and learning. *Open Online Course, INSA Toulouse, France*.

Montazem, A.-S., Garambois, P.-A., Calmant, S., Finaud-Guyot, P., Monnier, J., Medeiros Moreira, D., et al. (2019). Wavelet-based river segmentation using hydraulic control-preserving water surface elevation profile properties. *Geophysical Research Letters*, *46*(12), 6534–6543. https://doi.org/10.1029/2019GL082986

Nachtergaele, F., van Velthuizen, H., Verelst, L., Wiberg, D., Henry, M., Chiozza, F., et al. (2023). *Harmonized world soil database version 2.0*. FAO.

Oubanas, H., Gejadze, I., Malaterre, P.-O., & Mercier, F. (2018). River discharge estimation from synthetic swot-type observations using variational data assimilation and the full saint-venant hydraulic model. *Journal of Hydrology*, *559*, 638–647. https://doi.org/10.1016/j.jhydrol.2018.02.004

Paiva, R. C. D., Collischonn, W., Bonnet, M.-P., de Gonçalves, L. G. G., Calmant, S., Getirana, A., & Santos da Silva, J. (2013b). Assimilating in situ and radar altimetry data into a large-scale hydrologic-hydrodynamic model for streamflow forecast in the Amazon. *Hydrology and Earth System Sciences*, *17*(7), 2929–2946. https://doi.org/10.5194/hess-17-2929-2013

Paris, A., Dias de Paiva, R., Santos da Silva, J., Medeiros Moreira, D., Calmant, S., Garambois, P.-A., et al. (2016). Stage-discharge rating curves based on satellite altimetry and modeled discharge in the Amazon basin. *Water Resources Research*, *52*(5), 3787–3814. https://doi.org/10.1002/2014WR016618

Pavelsky, T. M. (2014). Using width-based rating curves from spatially discontinuous satellite imagery to monitor river discharge. *Hydrological Processes*, *28*(6), 3035–3040. https://doi.org/10.1002/hyp.10157

Pontes, P. R. M., Fan, F. M., Fleischmann, A. S., de Paiva, R. C. D., Buarque, D. C., Siqueira, V. A., et al. (2017). MGB-IPH model for hydrological and hydraulic simulation of large floodplain river systems coupled with open source GIS. *Environmental Modelling and Software*, *94*, 1–20. https://doi.org/10.1016/j.envsoft.2017.03.029

Pujol, L., Garambois, P.-A., Delenne, C., & Perrin, J.-L. (2024). Adjoint-based sensitivity analysis and assimilation of multi-source data for the inference of spatio-temporal parameters in a 2d urban flood hydraulic model. *Journal of Hydrology*, *643*, 131885. submitted. https://doi.org/10.1016/j.jhydrol.2024.131885

Pujol, L., Garambois, P.-A., Finaud-Guyot, P., Monnier, J., Larnier, K., Mosé, R., et al. (2020). Estimation of multiple inflows and effective channel by assimilation of multi-satellite hydraulic signatures: The ungauged anabranching Negro River. *Journal of Hydrology*, *591*, 125331. https://doi.org/10.1016/j.jhydrol.2020.125331

Pujol, L., Garambois, P.-A., & Monnier, J. (2022). *Multi-dimensional hydrological-hydraulic model with variational data assimilation for river networks and floodplains* (Vol. 2022, pp. 1–44). EGUsphere. https://doi.org/10.5194/egusphere-2022-10

Rodríguez, E., Durand, M., & Frasson, R. P. d. M. (2020). Observing rivers with varying spatial scales. *Water resources research*, *56*(9), e2019WR026476. https://doi.org/10.1029/2019WR026476

Roux, H. (2004). Estimation de paramètres en hydraulique fluviale, à partir de données caractéristiques de l'imagerie aérienne (Unpublished doctoral dissertation).

Samuels, P. G. (1989). Backwater lengths in rivers. *Proceedings–Institution of Civil Engineers*, *87*(4), 571–582. https://doi.org/10.1680/iicep.1989.3779

Schneider, R., Godiksen, P. N., Villadsen, H., Madsen, H., & Bauer-Gottwein, P. (2017). Application of Cryosat-2 altimetry data for river analysis and modelling. *Hydrology and Earth System Sciences*, *21*(2), 751–764. https://doi.org/10.5194/hess-21-751-2017

Schuite, J., Flipo, N., Massei, N., Rivière, A., & Baratelli, F. (2019). Improving the spectral analysis of hydrological signals to efficiently constrain watershed properties. *Water Resources Research*, *55*(5), 4043–4065. https://doi.org/10.1029/2018WR024579

Sobol', I., & Kucherenko, S. (2009). Derivative based global sensitivity measures and their link with global sensitivity indices. *Mathematics and Computers in Simulation*, *79*(10), 3009–3017. https://doi.org/10.1016/j.matcom.2009.01.023

Wongchuig-Correa, S., Cauduro Dias de Paiva, R., Biancamaria, S., & Collischonn, W. (2020). Assimilation of future swot-based river elevations, surface extent observations and discharge estimations into uncertain global hydrological models. *Journal of Hydrology*, *590*, 125473. https://doi.org/10.1016/j.jhydrol.2020.125473

Yamazaki, D., Ikeshima, D., Sosa, J., Bates, P. D., Allen, G. H., & Pavelsky, T. M. (2019). Merit hydro: A high-resolution global hydrography map based on latest topography dataset. *Water Resources Research*, *55*(6), 5053–5073. https://doi.org/10.1029/2019WR024873

Yoon, Y., Garambois, P.-A., Paiva, R. C., Durand, M., Roux, H., & Beighley, E. (2016). Improved error estimates of a discharge algorithm for remotely sensed river measurements: Test cases on Sacramento and Garonne rivers. *Water Resources Research*, *52*(1), 278–294. https://doi.org/10.1002/2015WR017319

Zanaga, D., Van De Kerchove, R., De Keersmaecker, W., Souverijns, N., Brockmann, C., Quast, R., et al. (2021). ESA world cover 10m 2020 v100. *Zenodo*. https://doi.org/10.5281/zenodo.5571936